UNIVERSITÀ DEGLI STUDI DI PADOVA

DIPARTIMENTO DI BIOLOGIA

Corso di Laurea in Biologia Molecolare

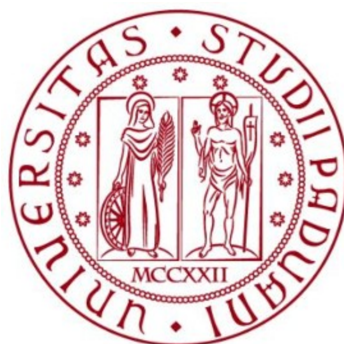

ELABORATO DI LAUREA

Come i macrofagi inducono tratti maligni nell'epitelio mammario attraverso le chinasi IKKε/TBK1 e la via della biosintesi della serina

Tutor: Prof. Luigi Leanza
Dipartimento di Biologia

Laureanda: Giada Ferrazzi

ANNO ACCADEMICO 2023/2024

INDICE

ABSTRACT *3*

1. STATO DELL'ARTE *5*

1.1 Il cancro al seno **5**

1.2 Ruolo dei macrofagi e dell'obesità **6**

1.3 Le chinasi IKKε/TBK1 e la via della serina **7**

2 APPROCCIO SPERIMENTALE *9*

2.1 modelli sperimentali **9**

2.1.1 Modelli in vitro: le colture cellulari 9

2.1.2 Differenziazione e polarizzazione dei macrofagi 9

2.1.3 Linee cellulari CRISPR 9

2.1.4 Modelli ex vivo: organoidi 10

2.1.5 Modelli in vivo: modello murino 10

2.2 Citometria a flusso **10**

2.3 Saggio di proliferazione e guarigione della ferita **10**

2.4 Western Blotting **11**

2.5 Saggio di Invasione 3D **11**

2.4 Saggio su agar morbido **12**

2.5 Immunofluorescenza **12**

2.6 Immunoistochimica **12**

2.7 Analisi dell'espressione genica **13**

2.8 Analisi Statistica **13**

3. RISULTATI *15*

3.1 Il terreno condizionato dai macrofagi induce la trasformazione tumorale **15**

3.2 Il terreno condizionato dai macrofagi induce proprietà maligne in sistemi modello primari murini e umani **18**

3.3 L'espressione di IKKε è associata all'infiammazione tumorale e media il fenotipo maligno indotto dal mezzo condizionato dai macrofagi **19**

3.4 NCT502, un inibitore della PHGDH, previene il fenotipo maligno indotto dal mezzo condizionato dai macrofagi **20**

3.5 Amlexanox ritarda la tumorigenesi *in vivo* in un modello murino di cancro al seno genetico combinato con l'obesità indotta dalla dieta **21**

4. DISCUSSIONE E CONCLUSIONI *23*

BIBLIOGRAFIA *25*

APPENDICE *26*

ABSTRACT

Il cancro al seno è il tumore più diffuso tra le donne e rappresenta una delle principali cause di decessi per cancro. Odierne ricerche hanno sottolineato l'impatto significativo dell'infiammazione cronica, legata in particolare all'obesità, nello sviluppo del carcinoma mammario. Questa tesi esamina le proprietà maligne acquisite dalle cellule epiteliali mammarie quando esposte ad un mezzo condizionato dai macrofagi ed il ruolo delle chinasi IKKε e TBK1, riconosciute per le loro attività oncogeniche nella tumorigenesi del seno, e la loro influenza sulla via biosintetica della serina (SBP), cruciale per il metabolismo delle cellule tumorali. Attraverso l'utilizzo di modelli sperimentali *in vitro*, *ex vivo* e *in vivo*, è stata analizzata la relazione tra obesità, macrofagi infiltranti e l'attivazione di IKKε nell'ambito del cancro al seno. Questi risultati suggeriscono che la sovra-regolazione di IKKε, innescata dall'infiltrazione di macrofagi nel tessuto adiposo mammario, potrebbe essere coinvolta nella progressione del tumore, indicando che la regolazione della via della serina potrebbe essere una terapia strategia per ridurre il rischio di cancro al seno nelle pazienti obese. Gli esiti di questo studio forniscono nuovi scenari per la creazione di terapie mirate che potrebbero migliorare le strategie di prevenzione, in particolare viene proposto l'utilizzo di amlexanox, farmaco approvato dalla FDA, per ridurre il rischio di cancro al seno associato all'obesità.

1. STATO DELL'ARTE

1.1 Il cancro al seno

Il seno femminile, localizzato nella parete toracica anteriore, è composto da pelle, tessuto sottocutaneo e tessuto mammario. Quest'ultimo comprende elementi parenchimali epiteliali e lo stroma. Ogni mammella è costituita da 15-20 lobi, i quali sono ulteriormente suddivisi in lobuli (da 20 a 40). Ciascun lobo è deputato alla produzione di latte e drena in un dotto galattoforo principale che giunge al capezzolo. Lo spazio tra i lobi è riempito da tessuto adiposo, deputato a proteggere il tessuto ghiandolare ed è fornito da una rete di nervi, vasi sanguigni, vasi linfatici, linfonodi e tessuto connettivo, il quale fornisce supporto strutturale. (1)
Il cancro al seno è il tumore più frequentemente diagnosticato nelle donne, in tutte le fasce di età, e si colloca al secondo posto tra le cause di morte per cancro nelle donne, con un'incidenza di circa una donna su 8 che si ammala di tumore della mammella in Italia. Generalmente, la tumorigenesi si verifica come risultato della disregolazione dei percorsi che controllano la proliferazione cellulare e l'apoptosi.
Il tumore si presenta comunemente come un nodulo nel seno ed è solitamente indolore. La maggior parte dei tumori al seno sono adenocarcinomi, con l'85% dei casi che derivano dai dotti galattofori e il 15% dall'epitelio lobulare.
La patologia duttale varia dal carcinoma duttale *in situ* ai carcinomi invasivi che si sono diffusi oltre la membrana basale nel parenchima mammario adiacente.
Per questo, una distinzione chiave può essere consolidata tra forme non invasive (si sviluppano dentro ai dotti) e forme che invece diventano invasive (possono propagarsi e invadere i tessuti circostanti).
Un' ulteriore classificazione dei diversi tipi di cancro al seno si basa sull'esistenza o mancanza di tre distinti recettori: il recettore degli estrogeni (ER+), il recettore del progesterone (PR+) ed il recettore 2 del fattore di crescita epidermico umano (HER2+). Se il tumore non esprime nessuno di questi tre recettori, viene identificato come cancro al seno triplo negativo (TNBC, più frequente nelle donne premenopausa) ed è solitamente più aggressivo rispetto agli altri, anche perché non è possibile utilizzare trattamenti ormonali o anticorpi monoclonali specifici per HER2.
Inoltre, diversi fattori, modificabili e non, sono associati a un rischio aumentato di sviluppare il cancro al seno. I fattori di rischio modificabili possono essere cambiati o evitati e includono l'obesità, uno stile di vita sedentario e l'esposizione a ormoni esogeni. Al contrario, fattori come la predisposizione genetica di una persona e l'invecchiamento non sono modificabili e sono inevitabili (2).
Una percentuale piuttosto bassa (circa il 5-10%) invece di tumori al seno è dovuta ad alterazioni nei geni BRCA-1 e BRCA-2. Questi geni, in condizioni normali, codificano per proteine capaci di correggere gli errori nel DNA. Tuttavia, quando questi geni risultano mutati, tali proteine non sono più in grado di sanare gli errori del DNA, i quali si accumulano portando all'insorgenza di un tumore.
I cambiamenti genetici possono essere ereditati da un genitore oppure possono manifestarsi naturalmente. In ogni caso possono essere trasmesse ai figli, ma è fondamentale precisare che non tutti coloro che sono portatori di una mutazione genica del BRCA-1 o del BRCA-2 evolvono un tumore alla mammella, ma tutti presentano una maggiore probabilità di rischio.

1.2 Ruolo dei macrofagi e dell’obesità

L'obesità è la seconda causa di cancro prevenibile dopo il fumo di tabacco ed è caratterizzata da uno stato infiammatorio cronico di basso grado.
In un individuo normopeso, il tessuto adiposo è caratterizzato da un ambiente anti-infiammatorio creato sia dalle cellule immunitarie residenti nel tessuto adiposo sia dagli adipociti.
Con l'eccesso cronico di nutrienti, tuttavia, gli adipociti cambiano il loro modello secretorio, rilasciando una serie di citochine e chemochine proinfiammatorie, come il fattore di necrosi tumorale alfa (TNF-α), l'interleuchina-6 (IL-6) e la proteina chemio-attrattiva dei monociti-1 (MCP-1). Questi segnali pro-infiammatori richiamano i macrofagi nel tessuto adiposo, i quali secernano mediatori infiammatori creando così un ambiente che promuove l’invasione del cancro e la metastasi.
I macrofagi sono definiti come i fagociti del sistema immunitario innato e svolgono un ruolo importante nella difesa dell'organismo, dalle infezioni e nel mantenimento dell'omeostasi tissutale. In generale, possono essere classificati in due fenotipi principali in base alle loro funzioni: il fenotipo M1 con risposte proinfiammatorie e funzioni antitumorali, mentre il fenotipo M2 è antinfiammatorio e promotore di tumori. Nelle fasi iniziali del cancro, i macrofagi associati al tumore (TAM) sono caratterizzati dal fenotipo M1 per attivare l'immunità antitumorale e inibire l'angiogenesi tumorale; esprimono alti livelli di IL-12 e basse di IL-10. Con la progressione del tumore verso stadi avanzati, i TAM vengono commutati al fenotipo M2 e facilitano l'angiogenesi con alti livelli di espressione di IL-10 e bassi livelli di IL-12 favorendo così la progressione tumorale. (2)

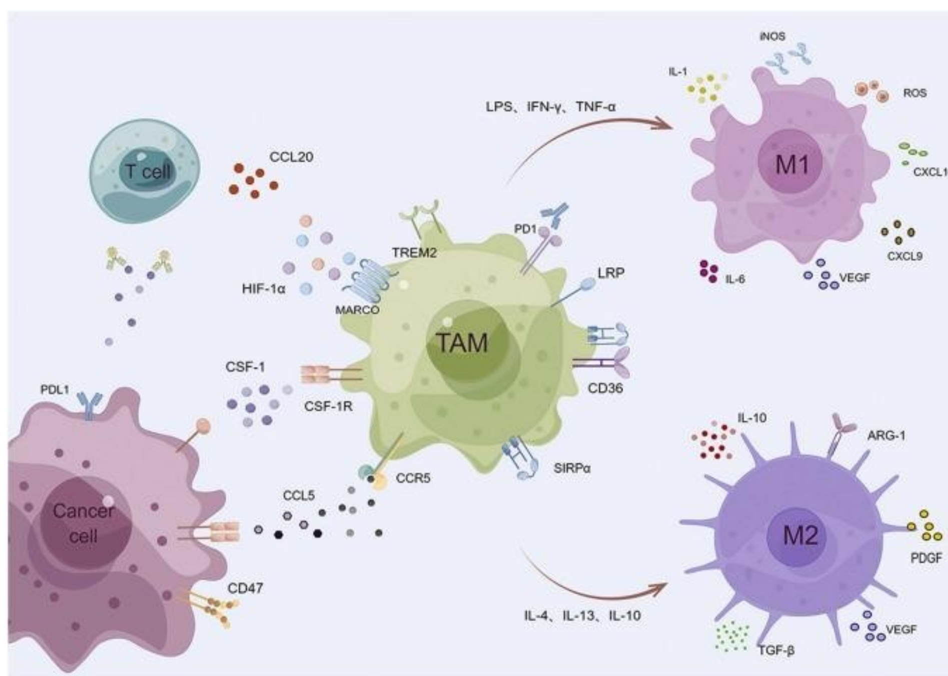

Fig.1 *I macrofagi cambiano il loro fenotipo e mostrano diverse caratteristiche funzionali sotto l’influenza dei segnali ambientali.*

I macrofagi infiltranti liberano il fattore di crescita dell'endotelio vascolare (VEGF) e il fattore di crescita trasformante beta (TGF-β), i quali possono stimolare la crescita delle cellule epiteliali mammarie e delle cellule cancerose.
L'obesità ed il rischio di cancro al seno presentano un rapporto complesso causato dal sottotipo e dallo stato di menopausa. L'obesità aumenta il rischio di TNBC nelle donne premenopausa, attraverso meccanismi infiammatori e metabolici, al contrario, nelle donne postmenopausa, incrementa il rischio di carcinoma mammario ER+ attraverso una maggiore produzione di estrogeni nel tessuto adiposo. Questi meccanismi sottolineano l'importanza di mantenere un peso corporeo sano per ridurre il rischio di diversi sottotipi di carcinoma mammario.

1.3 Le chinasi IKKε/TBK1 e la via della serina

Recentemente, tramite approcci di screening, sono state identificate due chinasi infiammatorie non canoniche della famiglia IKK, IKKε (Inhibitor of κB kinase epsilon) e TBK1 (TANK-binding kinase 1), le quali condividono un'identità di sequenza del 61% e svolgono ruoli oncogeni fondamentali nella tumorigenesi del seno.
Ancora più importante, i ruoli come oncogeni di IKKε e TBK1 non sono limitati solo all'attivazione dell'infiammazione e della risposta immunitaria innata mediante l'attivazione dei percorsi NF-κB (fattore di trascrizione che regola l'espressione di geni coinvolti nell'infiammazione e nella risposta immunitaria) e IRF3/7 (fattori di trascrizione che regolano la risposta antivirale e immunitaria), ma abilitano anche direttamente altri hub oncogenici come la chinasi AKT (proteina chinasi coinvolta in numerosi processi cellulari, tra cui la crescita cellulare, la sopravvivenza e il metabolismo che è spesso attivata in vari tipi di cancro) e il fattore trascrizionale YAP (regolatore trascrizionale che promuove la proliferazione cellulare e la sopravvivenza; è parte del *pathway* Hippo, importante nel controllo della crescita e della dimensione degli organi), in modo dipendente dalla fosforilazione, contribuendo alla tumorigenesi. (4)
Come riportato in precedenza, l'obesità provoca uno stato infiammatorio cronico che coinvolge la via di segnale NFκB, con un aumento persistente dei livelli di espressione sia di IKKε che di TBK1. Mentre il ruolo di TBK1 nel cancro al seno è controverso, IKKε è un oncogene del cancro al seno affermato, sovra-espresso nel 30% dei casi di cancro al seno. Oltre ad attivare l'infiammazione e la secrezione di citochine, si è dimostrato che IKKε regola il metabolismo cellulare, in particolare, la via di biosintesi della serina (SBP). L'SBP sostiene lo sviluppo delle cellule tumorali, in quanto le rifornisce di acidi grassi, di acidi nucleici e di proteine.
IKKε ha la capacità di controllare l'espressione di enzimi cruciali nella SBP, cambiando così il metabolismo cellulare e influenzando la crescita e la divisione delle cellule tumorali, mentre la SBP modula la produzione di citochine a valle di IKKε.
Nel 2011, due ricerche accertarono che PHGDH (fosfoglicerato deidrogenasi, primo enzima della via metabolica) può essere considerato come oncogene del cancro al seno e del melanoma. Recentemente è stato scoperto che il secondo enzima della via, PSAT1, viene regolato da IKKε.
Poiché IKKε può influenzare il metabolismo della serina, la modulazione di questa via potrebbe rappresentare una strategia terapeutica interessante per trattare il cancro al seno.

Dunque in questo studio è stata presa in considerazione l'ipotesi che durante l'obesità i macrofagi infiltrino il tessuto mammario provocando un aumento dell'espressione di IKKε, il quale, di conseguenza, contribuisce all'insorgenza del cancro al seno.
In questo modo è stato delineato un percorso di segnalazione che lega tra loro l'infiammazione e inizio del tumore ed una serie di inibitori che potrebbero ridurre il rischio di cancro al seno nei pazienti obesi.
Per ovviare ciò ci si è adoperati di diversi sistemi 3D, tra cui cellule MCF10A non trasformate, organi primari di topo e cellule epiteliali mammarie primarie umane.

2 APPROCCIO SPERIMENTALE

2.1 modelli sperimentali

2.1.1 Modelli in vitro: le colture cellulari

Le MCF10A sono una linea cellulare non trasformata che deriva dalle cellule epiteliali della ghiandola mammaria che viene ampiamente sfruttata nell'indagine biomedica. In questo studio sono state adoperate per esaminare i processi di trasformazione maligna e testare nuove terapie contro il cancro al seno. Sono state coltivate in sistemi 2D e 3D. Nei sistemi 2D le cellule vengono coltivate su una superficie piana e crescono a monostrato; nei sistemi 3D invece, crescono in una matrice tridimensionale dove le cellule formano strutture tridimensionali complesse che possono imitare la struttura degli organi e dei tessuti naturali.

2.1.2 Differenziazione e polarizzazione dei macrofagi

Tramite centrifugazione a gradiente di densità, sono state isolate le cellule mononucleate del sangue periferico umano (PBMC). Con questa tipologia di centrifugazione, le molecole sedimentano in un mezzo con densità crescente verso il basso; può essere isopicnica (le particelle si posizionano nella zona uguale alla loro densità) oppure zonale (sfrutta la diversa velocità con cui le particelle si muovono all'interno di un gradiente di densità in base alle differenze di forma e dimensione delle particelle).
Una volta fatte crescere su piastre, sono state differenziate in due gruppi principali di macrofagi sul terreno RPMI 1640 integrato col 10% di siero fetale bovino: M1D (utilizzando il fattore di crescita GM-CSF), considerati proinfiammatori e M2D (utilizzando il fattore di crescita MCSF) ritenuti invece antiinfiammatori.
Successivamente gli M1D sono stati attivati a M1A tramite l'impiego di 10 ng/ml di LPS e 20 ng/ml di IFN γ per 24 ore, mentre gli M2D sono stati attivati a M2A tramite 20 ng/ml di IL-4 per 48 ore.
Le quattro popolazioni cellulari (M1D, M1A, M2D, M2A) sono state caratterizzate tramite il metodo ELISA e array di citochine, rivelando che alcuni marcatori erano condivisi (come la secrezione di MCP1) mentre altri erano più specifici (TNFα per M1 e CCL22 per M2).
Per valutare i marcatori di espressione sulla superficie cellulare invece si è proceduti tramite analisi FACS, un tipo specializzato di citometria a flusso, permettendo così la caratterizzazione di diversi tipi di cellule in una miscela cellulare eterogenea.
Ciò che si è constatato è che le molecole M1D/A esprimevano livelli più elevati di HLA-DR mentre le molecole M2D/A alti livelli di CD86.

2.1.3 Linee cellulari CRISPR

Il sistema CRISPR-Cas9 è stato usufruito per trasfettare nelle cellule MCF10A, le quali esprimono stabilmente Cas9, crRNA IKKε, crRNA PHGDH o crRNA di controllo non mirato.
Le colonie in crescita sono state controllate per l'espressione di IKK ε o PHGDH tramite Western Blotting.

2.1.4 Modelli ex vivo: organoidi

Questa tecnologia permette di ricreare organi a partire da cellule staminali embrionali o pluripotenti in una coltura 3D, modellando fedelmente il comportamento e la funzione delle cellule *in vitro* ed *ex vivo.*

A partire da topi alimentati con una dieta ad alto contenuto di grassi (HFD) o con dieta normale (ND), sono stati ricavati organoidi mammari e seminati per colture 3D.

2.1.5 Modelli in vivo: modello murino

Impiego di topi femmine C57BI/6 eterozigoti per l'antigene middle T del poliomavirus. Il modello è stato impiegato per determinare se IKKε abbia un ruolo nella tumorigenesi indotta dall'obesità.

2.2 Citometria a flusso

È una metodica di laboratorio che consente un'analisi automatizzata di sospensioni cellulari monodisperse, misurando caratteristiche citologiche e/o biochimiche all'interno di un flusso laminare che interseca una sorgente luminosa, acquisendo e memorizzando più parametri (volume, fluorescenza, granularità) per ciascuna cellula acquisita.

Molto spesso viene chiamata citofluorimetria a flusso, in quanto prevede l'utilizzo di marcatori fluorescenti, come gli anticorpi che legano in modo specifico molecole presenti sulla superficie delle cellule di interesse.

Come riportato in precedenza, tale metodica è stata utilizzata per valutare i marcatori di espressione sulla superficie cellulare.

I macrofagi una volta colorati, sono stati lavati tre volte con PBS-/- ed incubati per 5 minuti per poi essere delicatamente lavati col buffer FACS.

I siti di legame non specifici sono stati bloccati con la soluzione di blocco dei recettori Fc e successivamente le cellule sono state co-colorate con anticorpi primari anti-HLA-DR coniugati con isotiocianato di fluoresceina, anti-CD86 coniugati con ficoeritrina-cianina 7, anti-CD163 coniugati con alloficocianina e anti-CD206 coniugati con PE per 30 minuti a 4°C al buio.

Le cellule sono state lavate due volte con il buffer FACS e colorate con DAPI per la separazione delle cellule vive/morte immediatamente prima dell'acquisizione dei dati sul citometro a flusso BD LSRFortessa 1.

I dati sono stati analizzati utilizzando il software FlowJo 10.6.1.

2.3 Saggio di proliferazione e guarigione della ferita

Il saggio di proliferazione è stato condotto tramite lo strumento IncuCyte ZOOM, il quale consente di monitorare e analizzare e colture cellulari in tempo reali, direttamente all'interno di un incubatore, osservando così la variazione del numero di cellule nel tempo, il numero di divisioni cellulari, l'attività metabolica.

Grazie ad esso si è potuto confermare che vi sono diversi meccanismi con cui i mezzi condizionati dai macrofagi influenzano la trasformazione e proliferazione.

Nel saggio di guarigione della ferita invece, la proliferazione è stata arrestata tramite trattamento con mitomicina C per due ore creano ferite con un WoundMaker a 96 pin.

WoundMarker è uno strumento utilizzato nella ricerca biologica, specificamente in esperimenti di migrazione cellulare o "wound healing" (guarigione delle ferite),

dove i 96 pin corrispondono ai 96 pozzetti della piastra, permettendo di creare una "ferita" in ogni pozzetto simultaneamente.
Infine la migrazione cellulare è stata identificata rilevando la confluenza cellulare nella zona della ferita per due giorni utilizzando sempre lo strumento IncuCyte ZOOM.
Questo saggio è stato utile per riportare parzialmente un tipico fenotipo maligno nelle colture 2D, ovvero la formazione di protrusioni invasive.

2.4 Western Blotting
È una tecnica che permette di trasferire macromolecole (ad esempio, le proteine) da un gel, in cui sia avvenuta la separazione elettroforetica, ad una membrana immobilizzata ("*blotting*"), fatta di nitrocellulosa o PVDF (polivinildifluoride).
Le proteine durante il trasferimento devono mantenere forma e struttura e la loro posizione dopo la corsa elettroforetica.
Dopo di che si procede con la saturazione ("*blocking*") della membrana per andare a coprire i siti aspecifici, tramite BSA al 4% oppure latte scremato, e si effettua una incubazione con anticorpi primari, e se necessario, anche secondari coniugati con un tracciante.
(La colorazione indiretta tramite anticorpo secondario è quella più usata, in quanto consente di amplificare il segnale).
La proteina target, in seguito a lavaggio, può essere rilevata ("*detection*") tramite fluorescenza, chemiluminescenza o metodiche colorimetriche.
In questo studio le proteine sono state separate tramite SDS-PAGE, trasferite su una membrana PVDF e sono state rilevate utilizzando anticorpi primari anti-IKKε, anti-TBK1, anti-PHGDH o anti-actina e la chemiluminescenza potenziata.
L'SDS-PAGE è detergente carico negativamente che ha la funzione di denaturare tutte le proteine conferendo una carica netta negativa, in modo da poterle separare solo sulla base della loro dimensione, mentre la chemiluminescenza è la luminescenza emessa nel corso di una reazione chimica. Si basa sulla reazione redox in cui il luminolo viene ossidato dal perossido di rafano (in presenza di H2O2) e libera luce.

2.5 Saggio di Invasione 3D
È un metodo sperimentale impiegato per analizzare la capacità delle cellule, in particolare quelle tumorali, di attraversare una matrice extracellulare in un contesto tridimensionale che riproduce in modo più realistico il microambiente naturale rispetto ai saggi bidimensionali tradizionali.
Le cellule MCF10A sono state seminate in Matrigel:Collagene I, dove il Matrigel (a basso contenuto di fattori di crescita, con concentrazione proteica tra 9 e 11 mg/ml) raffigura la membrana basale, mentre il collagene (concentrazione di 1.2 mg/ml) ritrae la matrice extracellulare stromale.
Al sedicesimo giorno, gli sferoidi MCF10A sono stati stimolati col terreno condizionato dai macrofagi o il terreno di controllo addizionato con 20 ng/ml di EGF, 500 ng/ml di idrocortisone e 10 μg/ml di insulina.
Per l'inibizione di IKK ε, il terreno è stato addizionato dall'inibitore specifico di IKKε/TBK1-amlexanox; per inibire la via di biosintesi della serina è stato usato l'inibitore PHGDH NCT502 e infine per inibire Rac è stato aggiunto NSC23766.
Questo saggio è stato utilizzato per studiare la metastasi e valutare il potenziale invasivo delle cellule tumorali, per analizzare l'efficacia di inibitori della

migrazione/invasione cellulare e per studiare i meccanismi molecolari coinvolti nella migrazione e invasione delle cellule.

2.4 Saggio su agar morbido

Cellule MCF10A, IKKε, PHGDH, sottoposte a knockout mediante CRISPR-Cas9, e cellule di controllo MCF10A CRISPR-Cas9 sono state seminate in agar morbido allo 0,4% in un mezzo condizionato da macrofagi per osservare la formazione di colonie con diametri superiori a 50 μm affermando così la capacità delle cellule di crescere in modo indipendente dall'ancoraggio (segno di trasformazione maligna).

2.5 Immunofluorescenza

Basata sull'interazione antigene-anticorpo, è una tecnica che permette di visualizzare le proteine o strutture cellulari sfruttando il fatto che ad un certo punto l'anticorpo si può accoppiare ad un fluoroforo.
Come per il Western blot, la marcatura può essere diretta (il fluoroforo si lega all'anticorpo primario) o indiretta (il fluoroforo si lega all'anticorpo secondario)
La tecnica è stata utilizzata per valutare un tratto distintivo della tumorigenesi precoce nel cancro al seno, ovvero lo spostamento delle cellule cancerose dalla loro nicchia di matrice normale e successivamente il riempimento dello spazio luminale delle strutture ghiandolari normalmente vuote, tramite due meccanismi possibili ovvero la fuga dall'arresto proliferativo e/o la traslocazione cellulare in combinazione con l'acquisizione di proprietà di sopravvivenza indipendente dall'ancoraggio.
Gli sferoidi MCF10A una volta colorati, sono stati lavati in PBS e fissati con PFA al 4% per 20 minuti a 37°C.
Successivamente sono stati risciacquati con PBS e permeabilizzati con Triton X-100 allo 0,5% per 10 minuti. Una volta permeabilizzati, sono stati lavati con FBS al 10% in buffer di immunofluorescenza e bloccati in buffer IF-FBS al 10% per saturare i siti di legame aspecifici.
In seguito, gli sferoidi sono stati incubati con anticorpi primari anti-laminina V coniugati con Alexa 488 o anti-Ki67 coniugati sempre con Alexa 488.
Fluoroforo utilizzato: Faloidina Alexa Fluor 633 che permette di marcare e visualizzare i filamenti di F-actina.
A differenza degli sferoidi MCF10A, gli organoidi sono stati incubati inizialmente con anticorpo anti-a-SMA in FBS-PBS al 10% durante la notte a 4% e dopo lavaggio, con anticorpo secondario coniugato con Alexa 488 e Alexa Fluor 633 phalloidin per un'ora.

2.6 Immunoistochimica

Permette di individuare in un campione di preparato istologico, la presenza di antigeni grazie al legame con un anticorpo specifico.
Il legame viene visualizzato mediante successive reazioni enzimatiche (tramite utilizzo di perossidasi o fosfatasi alcalina) che permettono di far precipitare un colorante, detto cromogeno, sul sito di legame tra l'anticorpo primario e l'antigene tissutale, rendendolo visibile.
I campioni di tessuto mammario sono stati ottenuti dalla BCI Breast Tissue Bank e tale metodo è stato impiegato per verificare l'associazione tra l'espressione di IKKε e l'infiammazione tumorale, ma non solo, anche per definire se la via biosintetica della serina sia associata al fenotipo maligno, andando ad analizzare il livello di

espressione della fosfoserina aminotransferasi 1 (PSTA1, secondo enzima della via SBP).
Per determinare l’espressione di IKKε, i campioni sono stati fissati in formalina al 10%, inclusi in paraffina, sezionati e fissati su vetrini e sottoposte all’immunoistochimica.
Il recupero dell'antigene è stato effettuato bollendo le sezioni di tessuto nel microonde in una soluzione di mascheramento dell'antigene a base di acido citrico, le quali poi sono state colorate per IKK ε con anticorpo anti-IKK ε C-terminale di coniglio, e la colorazione è stata visualizzata con la reazione DAB (diaminobenzidina, è un composto chimico comunemente utilizzato come substrato nella tecnica di immunoistochimica (IHC) per visualizzare la localizzazione di anticorpi marcati).
Per individuare invece l’espressione di PSTA1, le sezioni di tessuto sono state colorate con anti-PSTA1 di coniglio e la reazione è sempre stata visualizzata con reazione DAB.

2.7 Analisi dell’espressione genica

Si basa sull’utilizzo correlato del dataset di espressione genica METABRIC e l’analisi ESTIMATE, in modo da approfondire la comprensione del microambiente tumorale nel carcinoma mammario.
Il dataset METABRIC comprende dati di espressione genica per oltre 2.000 campioni di carcinoma mammario, essenziali per eseguire l'analisi ESTIMATE.
Quest’ultima invece utilizza i dati di espressione genica per calcolare i punteggi stromale, immunitario e di stima, che rappresentano la quantità di cellule stromali e immunitarie presenti nei campioni tumorali.

2.8 Analisi Statistica

È stato eseguito il test t di Student per valutare se la differenza tra i dati ottenuti da due gruppi (dipendenti o indipendenti) fossero statisticamente significative.
Per il confronto tra più di due gruppi, è stato eseguito un test post-hoc di Fisher LSD per l’analisi della varianza (ANOVA).
Invece, per i dati in vivo, il test log-rank è stato impiegato per determinare la significatività statistica nel numero di tumori sviluppati nel tempo.
L'espressione di IKKε nei carcinomi mammari è stata valutata tramite il test di Kruskal-Wallis con il test post-hoc di Dunn senza correzione.
Le associazioni tra l'espressione delle proteine e l'infiltrazione delle cellule immunitarie nei carcinomi mammari sono state analizzate usando la correlazione di Spearman.
Un valore di $P < 0,05$ è stato considerato indicativo di significatività statistica. Per concludere, l’analisi statistica è stata condotta con il software GraphPad Prism 8.0 o il software R.

3. RISULTATI

3.1 Il terreno condizionato dai macrofagi induce la trasformazione tumorale

Per analizzare l'azione dell'infiammazione sulle cellule epiteliali, come primo sistema modello si è deciso si avvalersi della linea cellulare mammaria non trasformata MCF10A.
Uno dei primi segni di trasformazione maligna è la capacità delle cellule di proliferare indipendentemente dall'adesione. Per valutare ciò, le cellule MCF10A sono state seminate in agar morbido e lasciate in coltura per 5 settimane.
In condizioni di controllo non si è verificata nessuna formazione di colonie, mentre i quattro terreni condizionati dai macrofagi (M1D, M1A, M2D, M2A) hanno stimolato la trasformazione delle cellule MCF10A, data la formazione di colonie dal diametro superiore ai 50 μm (*figura 2*).
Inoltre, tramite un saggio di proliferazione si è osservato che il mezzo condizionato dai macrofagi M1D, M2D e M2A ha incrementato anche il tasso di proliferazione. Al contrario invece, il mezzo condizionato dai macrofagi M1A ha avuto l'effetto opposto suggerendo sistemi diversi con cui influenzano la trasformazione e proliferazione.

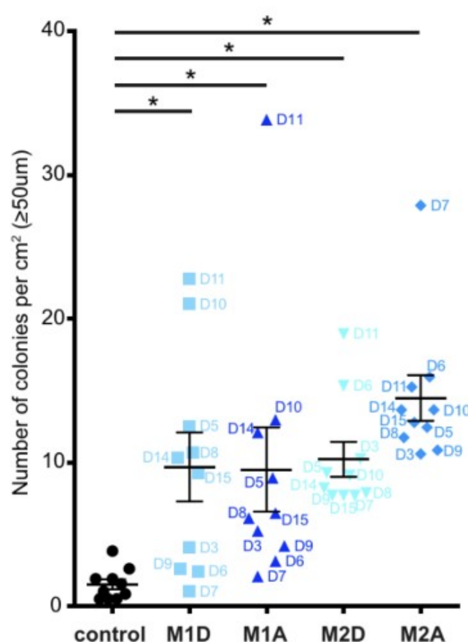

Figura 2: numero di colonie con diametro superiore ai 50 μm, indotte dai mezzi condizionati dai macrofagi per 25 donatori sani, ognuno etichettato con una lettera corrispondente D (D1-D25).

Questa differenza potrebbe essere indotta dalla differenza tra i sistemi 2D e 3D oppure per diversi tempi utilizzati negli esperimenti. Al contrario dei sistemi 2D, in quelli 3D, le cellule MCF10A formano acini che rispecchiano numerose caratteristiche dell'epitelio ghiandolare *in vivo* e sono valutati quindi un modello più idoneo per i seguenti esperimenti.

Un’altra comune caratteristica della tumorigenesi precoce nel cancro al seno, è il colmare dello spazio luminale delle strutture ghiandolari mammarie normalmente vuote.
Per affermarlo, i diversi terreni condizionati dai macrofagi sono stati applicati su acini di 16 giorni per 24 ore e come previsto, hanno provocato un incremento di acini con lume parzialmente o totalmente riempito e questo è dovuto ad una continua proliferazione e/o apprendimento di caratteristiche di sopravvivenza indipendente dall’ancoraggio (figura 3).
Tramite l’analisi dell’espressione di Ki67 mediante immunofluorescenza è stata testata la proliferazione, osservando un aumento solo nei mezzi condizionati da M1D e M1A (figura 4). È interessante notare che l’inibitore di Rac1 (la cui attivazione è implicata nella sopravvivenza indipendente dall’adesione) ha parzialmente impedito questo tipo di fenotipo in tutte le condizioni.

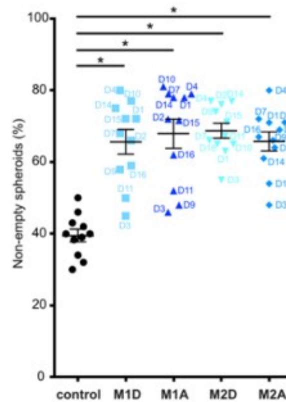

Figura 3: percentuale di acini con lume degli sferoidi parzialmente o completamente riempito, indotto dai mezzi condizionati dai macrofagi;

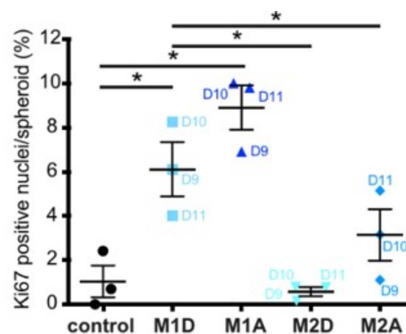

Figura 4: percentuale di nuclei positivi a Ki67 delle cellule MCF10A per sferoide;

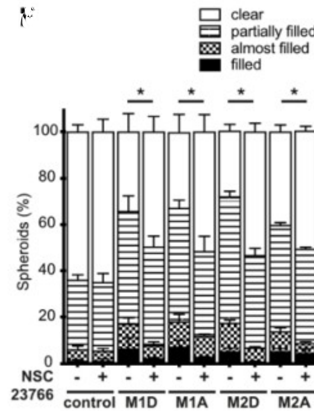

Figura 5: inibitore di Rac1, NSC23766, riduce il riempimento del lume degli sferoidi.

Ulteriore processo alla base della trasformazione maligna è la costituzione di protrusioni invasive con degradazione della laminina V riprodotto in tutti i mezzi condizionati dai macrofagi (*figura 6*). Tale effetto è stato impedito sempre tramite l'utilizzo dell'inibitore di Rac1, tranne nel mezzo condizionato da M1A.
Il fenotipo è stato ricreato anche in colture 2D, testando la migrazione delle cellule MCF10A in un saggio di guarigione delle ferite confermando che i mezzi condizionati da M1D, M2D, M2A hanno causato un tasso di migrazione più elevato e quello del mezzo M1A si è ridotto.

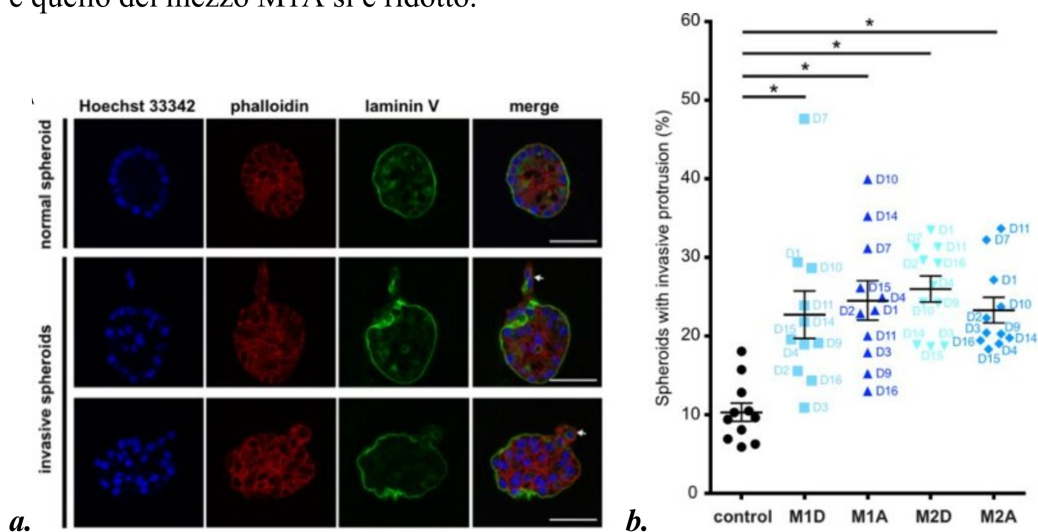

Figura 6: a. strutture 3D di sferoidi colorati per il DNA (Hoechst 3342, in blu), F-actina (falloidina, in rosso) e laminina V (verde); b. il mezzo condizionato dai macrofagi induce protrusioni invasine negli sferoidi MCF10A.

In sintesi, questi risultati hanno mostrato che i terreni condizionati da macrofagi provenienti da donatori sani favoriscono l'acquisizione di caratteristiche maligne chiave, come la crescita indipendente dall'ancoraggio e l'invasività, nelle cellule epiteliali mammarie non tumorali MCF10A coltivate in 3D.

3.2 Il terreno condizionato dai macrofagi induce proprietà maligne in sistemi modello primari murini e umani

Il terreno condizionato dai macrofagi M1A e M2A (M1D e M2D non sono stati testati), hanno indotto la formazione di protrusioni invasive anche negli organoidi primari di topo allevati tramite una dieta normale. Questo è stato messo in evidenza tramite la colorazione per α-SMA, che ha evidenziato la perdita della normale struttura a doppio strato composta da cellule mioepiteliali basali e cellule epiteliali luminali interne (*figura 7*).

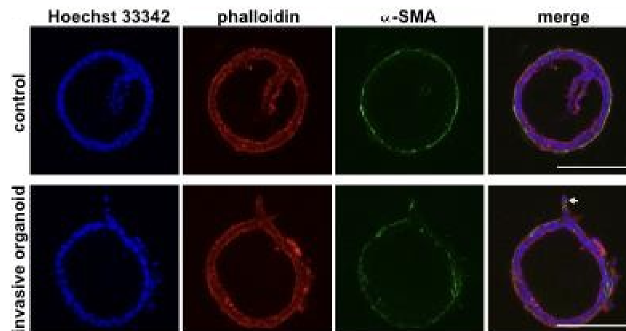

Figura 7: struttura 3D degli organoidi colorati per il DNA (Hoechst 33342, in blu), F-actina (falloidina, in rosso) e αSMA (verde).

Nelle prime fasi dell'obesità, i macrofagi infiltrano il tessuto mammario e si pensa che causino bassi livelli di infiammazione cronica locale.
Poiché questi risultati sono stati riportati in un modello di sovralimentazione nei topi, si è studiato il comportamento invasivo degli organoidi mammari primari di topi provenienti da animali nutriti con una dieta ricca di grassi (HFD) e una dieta normale (ND).
Una volta coltivati in collagene, si è potuto dimostrare che gli organoidi derivati da topi nutriti con dieta HFD sono più invasivi, osservando un numero maggiore di macrofagi infiltranti (*figura 8*).

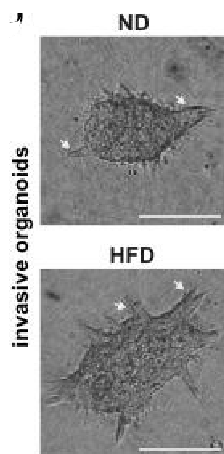

Figura 8: immagine rappresentative di organoidi coltivati in collagene per 2 giorni.

Inoltre, è essenziale sottolineare che cellule mioepiteliali e luminali umane isolate da una riduzione mammoplastica se coltivate in terreni condizionati dai macrofagi M1A e M2A, riproducono il carcinoma duttale in situ con riempimento del lume e ricostituzione delle strutture a doppio strato (*figura 9*).

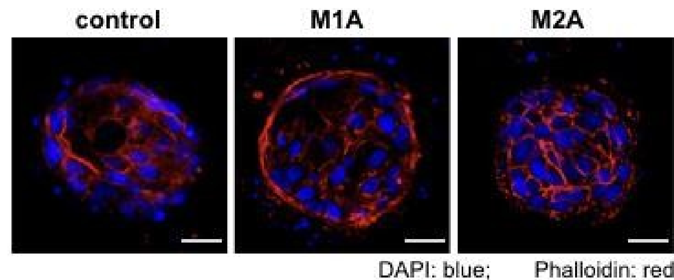

Figura 9: immagini rappresentative delle strutture duttali coltivate in mezzi condizionati da macrofagi M1A e M2A; i dotti sono stati colorati per il DNA (DAPI, in blu) e F-actina (falloidina, in rosso).

3.3 L'espressione di IKKε è associata all'infiammazione tumorale e media il fenotipo maligno indotto dal mezzo condizionato dai macrofagi

Per provare che l'espressione di IKKε nel cancro al seno sia associata all'infiltrazione immunitaria, è stata attuata un'analisi semi-quantitativa tramite immunoistochimica in una coorte di 66 carcinomi mammari umani.
Quello che si è potuto riscontrare è che nell'83% dei casi, IKK ε era espressa a medio o alto livello, comprovando una solida correlazione col grado di infiammazione (*figura 10a*).
Anche l'analisi trascrittomica del dataset del cancro al seno METABRIC ha dimostrato che i livelli di trascrizione dell'mRNA di IKBKE ed il pattern di espressione genica associato all'infiltrazione immunitaria (immuno score, ESTIMATE) sono fortemente correlati (*figura 10b*).

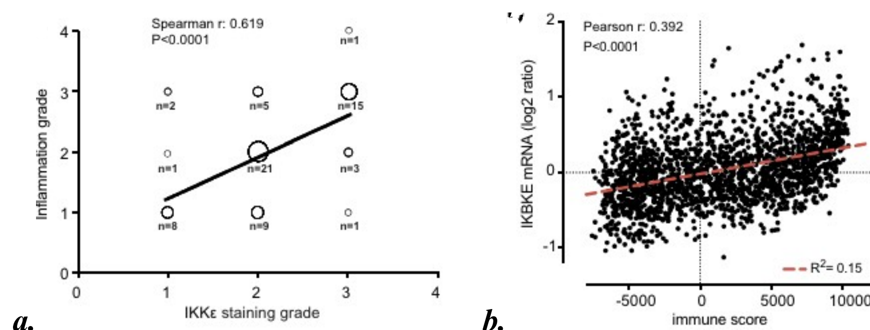

Figura 10: a. correlazione tra l'espressione di IKK εe l'infiltrazione delle cellule immunitarie ("0": nessuna cellula infiammatoria; "1": debole; "2": moderata; "3": forte; "4": molto forte). La dimensione dei cerchi mostra il numero di tumori rientranti nella categoria.
b. correlazione tra i livelli di mRNA di IKBKE (rapporto log2) e quelli della risposta immunitaria nel dataset trascrittomico METABRIC di 1981 pazienti con cancro al seno.

Per attestare il ruolo funzionale di IKKε nella trasformazione mediata dai macrofagi, ci si è avvalsi dell'inibitore di IKKε/TBK1, amlexanox, un farmaco accolto dalla FDA e precedentemente adoperato per trattare le ulcere orali.
Quando 50 μM di amlexanox vengono addizionati ai terreni condizionati dai macrofagi applicati alle cellule MCF10A, vi è una potente inibizione di tutte le caratteristiche relative alla trasformazione maligna.
Inoltre risultano diminuiti il numero di organoidi con protrusioni invasive derivati da topi con dieta normale o ad alto contenuto di grassi ed il riempimento del lume è stato inibito anche nel sistema modello umano.
Se il gene IKBKE, che codifica per IKK ε viene eliminato nelle cellule MCF10A tramite la tecnologia CRISPR-Cas9, si osserva una riduzione di colonie quando le cellule MCF10A vengono coltivate in agar morbido con medium condizionati dai macrofagi e non sono riuscite a formare protrusioni invasive quando piantate in una miscela di Matrigel/collagene.

3.4 NCT502, un inibitore della PHGDH, previene il fenotipo maligno indotto dal mezzo condizionato dai macrofagi

La fosfoglicerato deidrogenasi, il primo enzima della via di biosintesi della serina (SBP), quando sovraespresso negli sferoidi MCF10A, induce la creazione di sferoidi disorganizzati con lume riempito. Per consolidare se questa via è collegata al fenotipo infiammatorio nel cancro al seno, prima si è esaminato il livello di espressione del secondo enzima della via, PSAT1, ultimamente scoperto essere regolato da IKKε (come PHGDH).
Quello che si è visto è che nel 71% dei casi la proteina era espressa a livello medio o alto (*figura 11*) e vi è una forte correlazione tra l'espressione di PSTA1 e i livelli di IKKε, indicando quindi una correlazione tra infiammazione e SBP nei tumori al seno.

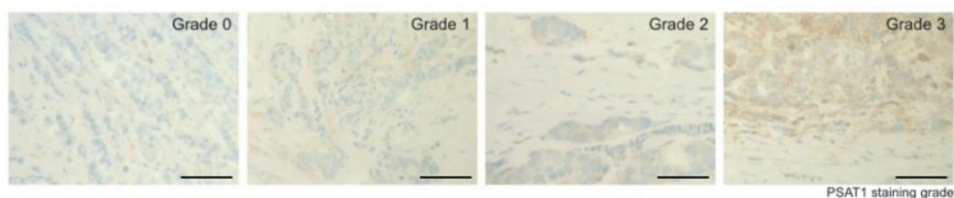

Figura 11: l'espressione di PSTA1 è stata valutata semi-quantitativamente utilizzando una scala di gradi crescente da 0 a 3 su sezioni di cancro al seno umano mediante immunoistochimica.

Per verificare l'ipotesi che l'attivazione della SBP a valle di IKK ε potrebbe contribuire all'acquisizione di proprietà maligne nelle cellule MCF10A, l'inibitore NCT502 è stato addizionato ai terreni condizionati dai macrofagi.
Similmente ad amlexanox, NCT502 ha impedito o ridotto la comparsa di un fenotipo maligno, quali crescita indipendente dall'ancoraggio, riempimento del lume, formazione di protrusioni invasive.
Inoltre i mezzi condizionati dai macrofagi non hanno riprodotto alcun fenotipo nelle cellule MCF10A in cui il gene PHGDH fosse stato rimosso tramite CRISPR-Cas9.

3.5 Amlexanox ritarda la tumorigenesi *in vivo* in un modello murino di cancro al seno genetico combinato con l'obesità indotta dalla dieta

È stato impiegato il modello murino di cancro al seno che porta una copia eterozigote del virus dei tumori mammari murino-antigene middle T del poliomavirus, per esaminare se IKK ε è coinvolto nella tumorigenesi indotta dall'obesità.
Dieci topi femmine hanno iniziato la dieta ad alta percentuale di grassi prima dello sviluppo del tumore mammario ed insieme a topi di controllo con dieta normale sono stati trattati quotidianamente con amlexanox.
È stato incluso anche un gruppo di controllo (topi *wild-type*) per confermare l'efficacia della dieta e per controllare eventuali interazioni impreviste del gene MMTV-PyMT. Sia i topi *wild-type* che MMTV-PyMT alimentati con dieta ricca di grassi, guadagnano più peso rispetto a quelli alimentati con una dieta normale.
Inoltre, la latenza dei tumori è stata considerevolmente diminuita dalla dieta HFD nei topi MMTV-PyMT.
I risultati riportati nella figura 12 hanno dimostrato che Amlexanox non influisce sullo sviluppo dei tumori nei topi MMTV-PyMT alimentati con la dieta normale ma ritarda la formazione dei tumori invece nei topi alimentati con la dieta ricca di grassi. Possiamo affermare quindi che l'obesità indotta in maniera sinergica dalla dieta con MMTV-PyMT nella promozione della formazione dei tumori.

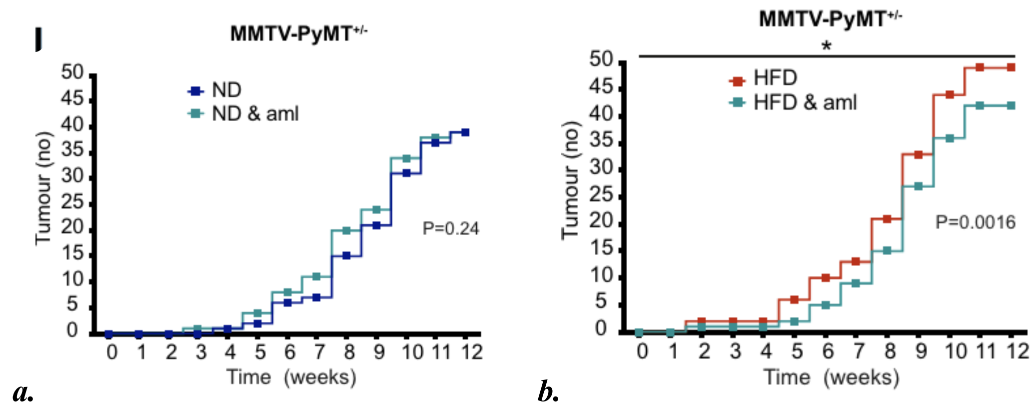

Figura 12: a. l'amlexanox non influisce sullo sviluppo dei tumori nei topi MMTV-PyMT con dieta ND ma b. ritarda la formazione dei tumori in topi HFD.

4. DISCUSSIONE E CONCLUSIONI

In questo studio è stato analizzato il ruolo cruciale dei macrofagi nella progressione delle prime fasi di trasformazione maligna a livello tissutale, essendo protagonisti nel provocare un'infiammazione cronica di basso grado, uno dei principali motivi responsabile del maggior rischio di cancro al seno associato all'obesità.
A prescindere dalla loro attivazione, i quattro mezzi condizionati dai macrofagi, derivati da donatori sani, hanno indotto la comparsa di proprietà maligne grazie alla loro attività secretoria, attraverso meccanismi differenti finora scarsamente caratterizzati.
Attualmente è stato comprovato che i macrofagi presenti nelle mammelle delle donne obese mostrano similarità coi macrofagi associati al tumore (TAM) ed assomigliano maggiormente ai macrofagi M2 data la riprogrammazione metabolica dovuta alla loro attività pro-tumorigenica.
Tuttavia, dato che l'estensione dei macrofagi attorno agli adipociti morti (chiamate strutture a corona) è associata ad un aumento di citochine pro-infiammatorie nella circolazione, anche questi macrofagi sono considerati M1.
In sintesi, è importante considerare che i macrofagi sono una popolazione eterogenea con M1 e M2 che rappresentano degli estremi semplificati.
Analogamente, restano da chiarire i ruoli di altre cellule immunitarie, così come degli adipociti e di altri tipi di cellule stromali (ad esempio, fibroblasti), nella penetrazione del tessuto mammario *in vivo*.
I dati suggeriscono che i macrofagi, attraverso la secrezione di citochine e altri mediatori infiammatori, creano un ambiente favorevole per l'attivazione di IKKε e TBK1 nelle cellule epiteliali.
Questo fenomeno sottolinea l'importanza dell'interazione cellula-cellula nel microambiente tumorale, dove i macrofagi non sono solo semplici effettori dell'infiammazione, ma attori attivi nel promuovere la progressione tumorale.
Ciononostante l'acquisizione delle caratteristiche maligne possono essere prevenute tramite inibizione genetica di IKKε e PHGDH col metodo CRISPR/Cas9 oppure farmacologicamente grazie al farmaco amlexanox (inibitore delle chinasi IkB non canoniche IKK ε e TBK1) e NCT502 (inibitore di PHGDH).
Infatti l'identificazione delle chinasi IKKε e TBK1 come mediatori centrali e la scoperta che IKKε svolge un ruolo centrale nella regolazione della via di biosintesi della serina (SBP), influenzando così la proliferazione e la sopravvivenza delle cellule tumorali, suggerisce nuove potenziali vie terapeutiche mirate per contrastare la malignità indotta dai macrofagi senza compromettere la loro funzione immunitaria difensiva.
Amlexanox è un farmaco approvato dalla FDA (Food and Drug Administration), un potente inibitore delle chinasi, che blocca la fosforilazione di varie proteine e questi effetti sono all'origine di reazioni antitumorali, antifibrotici e immunomodulatori. È attualmente impiegato contro le ulcere aftose e recentemente testato in pazienti obesi con diabete di tipo 2 e steatosi epatica non alcolica, dove ha portato ad un riscontro positivo nei parametri metabolici.
Inoltre l'almexanox è un farmaco interessante perché offre la possibilità di indurre l'inibizione sia della crescita del tumore che del dolore associato al tumore, frequente nei pazienti con melanoma. (5)

Da questa ricerca si può dedurre che amlexanox ha avuto un effetto preventivo diretto dell'infiammazione. Infatti quando aggiunto ai mezzi condizionati dai macrofagi applicati alle cellule MCF10A ha inibito tutte le caratteristiche maligne, come la crescita indipendente dall'ancoraggio, il riempimento del lume degli sferoidi e la formazione di protrusioni invasive.
Ha ridotto il numero di protrusioni invasive negli organoidi primari mammari di topi derivati da una dieta normale e dieta ad alto contenuto di grassi.
Inoltre il riempimento del lume è stato inibito anche nel sistema modello umano ed infine ha ritardato la formazione di tumori *in vivo* in un modello combinato di obesità indotta da dieta/cancro al seno MMTV-PyMT.
Altra scoperta fondamentale è che l'attivazione della via della serina, a valle di IKKε, è essenziale per l'acquisizione dei fenotipi maligni indotti dai mezzi condizionati dai macrofagi.
Grazie alla scoperta dell'inibitore NCT502, analogamente come amlexanox, esso ha prevenuto la crescita indipendente dall'ancoraggio, il riempimento del lume, ha ridotto il numero di protrusioni invasive negli organoidi primari mammari di topi alimentati con dieta normale e dieta HFD. Inoltre, è stata osservata la sua efficacia *in vivo* nel ridurre la crescita dei tumori che sovra-esprimono PHGDH.
I risultati di questa ricerca aprono nuove prospettive per lo sviluppo di trattamenti personalizzati che tengano conto dello stato metabolico e infiammatorio del paziente.
Futuri studi saranno necessari per approfondire ulteriormente i meccanismi molecolari alla base dell'interazione tra IKKε, metabolismo della serina e obesità, e per valutare l'efficacia di nuovi inibitori mirati in contesti clinici.
Pertanto, il targeting di queste chinasi potrebbe rappresentare una strategia efficace per limitare la progressione tumorale, aprendo la strada a sviluppi terapeutici che potrebbero migliorare significativamente le prospettive per i pazienti affetti da carcinoma mammario.

BIBLIOGRAFIA

1. Pandya S, Moore RG. Breast development and anatomy. Clin Obstet Gynecol. 2011 Mar;54(1):91-5. doi: 10.1097/GRF.0b013e318207ffe9. PMID: 21278507.
2. Katsura C, Ogunmwonyi I, Kankam HK, Saha S. Breast cancer: presentation, investigation and management. Br J Hosp Med (Lond). 2022 Feb 2;83(2):1-7. doi: 10.12968/hmed.2021.0459. Epub 2022 Feb 7. PMID: 35243878.
3. Munir MT, Kay MK, Kang MH, Rahman MM, Al-Harrasi A, Choudhury M, Moustaid-Moussa N, Hussain F, Rahman SM. Tumor-Associated Macrophages as Multifaceted Regulators of Breast Tumor Growth. Int J Mol Sci. 2021 Jun 18;22(12):6526. doi: 10.3390/jms22126526. PMID: 34207035; PMCID: PMC8233875.
4. Xie W, Jiang Q, Wu X, Wang L, Gao B, Sun Z, Zhang X, Bu L, Lin Y, Huang Q, Li J, Guo J. IKBKE phosphorylates and stabilizes Snail to promote breast cancer invasion and metastasis. Cell Death Differ. 2022 Aug;29(8):1528-1540. doi: 10.1038/s41418-022-00940-1. Epub 2022 Jan 22. PMID: 35066576; PMCID: PMC9345937.
5. Bailly C. The potential value of amlexanox in the treatment of cancer: Molecular targets and therapeutic perspectives. Biochem Pharmacol. 2022 Mar;197:114895. doi: 10.1016/j.bcp.2021.114895. Epub 2021 Dec 28. PMID: 34968491.

APPENDICE

Wilcz-Villega E, Carter E, Ironside A, Xu R, Mataloni I, Holdsworth J, Jones W, Moreno Béjar R, Uhlik L, Bentham RB, Godinho SA, Dalli J, Grose R, Szabadkai G, Jones L, Hodivala-Dilke K, Bianchi K. Macrophages induce malignant traits in mammary epithelium via IKKε/TBK1 kinases and the serine biosynthesis pathway. EMBO Mol Med. 2020 Feb 7;12(2):e10491. doi: 10.15252/emmm.201910491. Epub 2020 Jan 13. PMID: 31930708; PMCID: PMC7005540.

Article

Check for updates

EMBO
Molecular Medicine

Macrophages induce malignant traits in mammary epithelium via IKKe/TBK1 kinases and the serine biosynthesis pathway

Ewa Wilcz-Villega[1], Edward Carter[2,†], Alastair Ironside[2,†], Ruoyan Xu[1,†], Isabella Mataloni[1], Julie Holdsworth[2], William Jones[1], Rocío Moreno Béjar[1], Lukas Uhlik[1], Robert B Bentham[3], Susana A Godinho[1], Jesmond Dalli[4], Richard Grose[2], Gyorgy Szabadkai[3,5,6], Louise Jones[2], Kairbaan Hodivala-Dilke[2] & Katiuscia Bianchi[1,*]

Abstract

During obesity, macrophages infiltrate the breast tissue leading to low-grade chronic inflammation, a factor considered responsible for the higher risk of breast cancer associated with obesity. Here, we formally demonstrate that breast epithelial cells acquire malignant properties when exposed to medium conditioned by macrophages derived from human healthy donors. These effects were mediated by the breast cancer oncogene IKKe and its downstream target—the serine biosynthesis pathway as demonstrated by genetic or pharmacological tools. Furthermore, amlexanox, an FDA-approved drug targeting IKKe and its homologue TBK1, delayed in vivo tumour formation in a combined genetic mouse model of breast cancer and high-fat diet-induced obesity/inflammation. Finally, in human breast cancer tissues, we validated the link between inflammation–IKKe and alteration of cellular metabolism. Altogether, we identified a pathway connecting obesity-driven inflammation to breast cancer and a potential therapeutic strategy to reduce the risk of breast cancer associated with obesity.

Keywords inflammation; macrophages; malignant transformation; obesity; tumour metabolism
Subject Categories Cancer; Immunology; Metabolism
DOI 10.15252/emmm.201910491 | Received 21 February 2019 | Revised 3 December 2019 | Accepted 4 December 2019 | Published online 13 January 2020
EMBO Mol Med (2020) 12: e10491

Introduction

Obesity is a known risk factor for triple-negative breast cancer in pre-menopausal women (Yang et al, 2011) and for oestrogen receptor-positive (ER^+) breast cancer in post-menopausal women (Agnoli et al, 2010). The mechanism responsible for obesity-associated cancer risk is not well established. While the systemic effects of obesity, such as insulin resistance and dysregulated steroid hormones, have been studied extensively, less is known about the local consequences of obesity. In obese women, macrophages infiltrate the breast tissue in the absence of tumours (Sun et al, 2012), and both in humans and in mouse models of obesity, the presence of crown structures, consisting of macrophages and necrotic adipocytes, has been reported (Morris et al, 2011; Subbaramaiah et al, 2011). Macrophages are recruited and activated by monocyte chemoattractant protein 1 (MCP1, also known as CCL2), secreted by adipocytes during obesity, and are necessary for tumour progression (Arendt et al, 2013); accordingly, loss of MCP1 delays mammary tumourigenesis in a triple-negative breast cancer model (Cranford et al, 2017). Macrophages are thus crucial players in inducing the low level of chronic inflammation associated with obesity that has been proposed to drive malignant transformation at the tissue level (Olson et al, 2017), raising the possibility that anti-inflammatory drugs could be used to reduce breast cancer recurrence (Bowers et al, 2014). However, obesity-associated inflammation also leads to increased angiogenesis (Arendt et al, 2013) and alters extracellular matrix stiffness (Seo et al, 2015). In conclusion, the cellular mechanisms by which macrophage-mediated inflammation promotes malignant transformation are poorly characterized.

1 Centre for Molecular Oncology, Barts Cancer Institute, John Vane Science Centre, Queen Mary University of London, London, UK
2 Centre for Tumour Biology, Barts Cancer Institute, John Vane Science Centre, Queen Mary University of London, London, UK
3 Department of Cell and Developmental Biology, Consortium for Mitochondrial Research, University College London, London, UK
4 Lipid Mediator Unit, Biochemical Pharmacology, William Harvey Research Institute, Barts and the London School of Medicine, Queen Mary University of London, London, UK
5 Francis Crick Institute, London, UK
6 Department of Biomedical Sciences, University of Padua, Padua, Italy
*Corresponding author. Tel: +44 (0)20 7882 2049; E-mail: k.bianchi@qmul.ac.uk
†These authors contributed equally to this work

© 2020 The Authors. Published under the terms of the CC BY 4.0 license

Downloaded from https://www.embopress.org on April 18, 2024 from IP 147.162.3.230.

Interestingly, the non-canonical members of the IKK family, IjB kinase e (IKKe) and TANK binding kinase 1 (TBK1) are overexpressed in the white adipose tissue of mice on high-fat diet (HFD) (Chiang et al, 2009; Zhao et al, 2018) and IKKe is induced as a consequence of macrophage infiltration (Sanada et al, 2014). While the role of TBK1 in breast cancer is controversial (Yang et al, 2013; Deng et al, 2014), IKKe is an established breast cancer oncogene, overexpressed in 30% of breast cancer cases (Boehm et al, 2007). IKKe was originally identified as key mediator of the innate immune response (tenOever et al, 2007) and is also known as inducible IKK (IKK-i), being upregulated by several cytokines, e.g. TNF-a, IL6 and IFNc (Shimada et al, 1999). The IKBKE gene is located on chromosome 1q, which is frequently amplified in breast cancer, partly explaining overexpression of the kinase. However, in around 50% of the cases, the IKBKE transcript is increased (> 2-fold) even in the absence of copy-number changes in its chromosomal region 1q32 (Boehm et al, 2007). Interestingly, in triple-negative breast cancer cell lines without amplification of the IKBKE gene locus, IKKe expression is induced by cytokines, indicating that inflammation could be responsible for IKKe overexpression in the absence of genetic alterations (Barbie et al, 2014).

We thus postulated that during obesity, macrophage infiltration in the breast induces IKKe expression, ultimately contributing to malignant transformation. We show that medium conditioned by macrophages derived from 25 human healthy donors induces acquisition of a malignant phenotype in different 3D systems: (i) the non-transformed MCF10A cells, (ii) mouse primary organoids and (iii) human primary breast epithelial cells derived from patients. Moreover, using pharmacological tools and CRISPR-Cas9 technology, we demonstrate that inhibition of IKKe and its downstream signalling prevents this phenotype. Finally, we show that amlexanox, an FDA-approved drug targeting IKKe and its homologue TBK1, delays tumour appearance in vivo in a combined genetic mouse model of breast cancer and diet-induced obesity. Thus, we have described a signalling pathway linking inflammation and cancer initiation and have identified inhibitors with the potential to reduce the risk of breast cancer in obese patients.

Results

Macrophage-conditioned medium induces acquisition of malignant properties

To investigate the consequences of macrophage infiltration in the breast tissue, we used medium conditioned by human peripheral blood mononuclear cells (PBMCs) differentiated and activated as described below. Macrophages show a wide range of phenotypes, influenced by the surrounding microenvironment, but the spectrum of different phenotypes can be characterized into two major groups, such as the classically activated M1 (considered as pro-inflammatory) and alternatively activated M2 macrophages (considered as anti-inflammatory; Murray & Wynn, 2011). We used (i) GM-CSF to induce the differentiation of monocytes to M1-like macrophages (M1D) that were then activated with LPS/IFNc (M1A) and (ii) M-CSF to induce the differentiation to M2-like macrophages (M2D) that were then activated with IL-4 (M2A) (Fig EV1A). PBMCs were isolated from 25 healthy donors (Fig EV1A–D), and each donor was labelled with a corresponding letter D (D1–D25), to follow the correlation between each donor and the induced phenotypes. Characterization of the four cell populations via ELISA and cytokine array showed that some markers were shared, such as secretion of MCP1 (Fig EV1E and F), while others were more specific for M1A such as secretion of TNF-a (Fig EV1C), MIG and RANTES (Fig EV1E, G, H) or M2, such as secretion of CCL22 (M2A) (Fig EV1D), IL-10 and TGF-b1 (M2D/A) (Fig EV1E, I, J) (Table EV1). With regard to expression markers known to be induced by certain stimuli (Georgouli et al, 2019) (and associated with certain macrophage subgroups), we observed by FACS analysis that the majority of the cells in the four populations were double-positive for HLA-DR/CD86 (Fig EV2A and B), with M1D/A expressing HLA-DR at higher level than M2A/D (Fig EV2C), while CD86 was higher in M1A and M2A than in M1D and M2D (Fig EV2D). The percentage of cells double positive for CD206/CD163 was higher in the M2D/A populations (Fig EV2E and F), and CD206 was expressed at higher level by M1D and M2A, while CD163 by M2D/A (Fig EV2G and H).

To evaluate the effect of inflammation on epithelial cells, we decided to use the non-transformed breast epithelial cell line MCF10A, as first model system of receiving cells. The ability of cells to grow in an anchorage-independent manner is considered a sign of malignant transformation (Borowicz et al, 2014); thus, we seeded MCF10A cells in soft agar and monitored colony formation over a period of 5 weeks. As a control, we used medium recycled from MCF10A cells themselves, which was compared to media conditioned by M1-differentiated (M1D), M1-activated (M1A), M2-differentiated (M2D) and M2-activated (M2A) macrophages (Fig EV1A and Table EV1). As expected, in control conditions we did not observe any colony formation; however, the four macrophage-conditioned media-induced transformation of MCF10A cells as demonstrated by the presence of colonies with diameters exceeding 50 lm (Fig 1A and EV3A).

We then tested the effect of the macrophage-conditioned media using a standard proliferation assay and observed that M2A, together with M2D and M1D macrophage-conditioned media, also enhanced MCF10A proliferation rate in 2D, but the medium conditioned by M1A macrophages had the opposite effect (Fig EV3B and C), indicating separate mechanisms by which the macrophage-conditioned media affect transformation and proliferation. These discrepancies could be due to the differences between 2D and 3D systems, as previously reported for Ha-Ras and Her2 (Janda et al, 2002), or to different timeframes used in the experiments.

When cultured in 3D conditions, MCF10A cells form acini recapitulating numerous features of the glandular epithelium in vivo (Debnath & Brugge, 2005) and therefore are considered as a physiologically more appropriate model to monitor alterations associated with different stages of tumourigenesis. Thus, in the following experiments, we used this model system to understand the effect of macrophages on epithelial cells.

A hallmark of early tumourigenesis in breast cancer is the displacement of cancer cells from their normal matrix niche and subsequently filling the luminal space of the normally hollow glandular structures (Schafer et al, 2009). To confirm the transforming properties of the different media conditioned by macrophages, we applied them on 16-day-old acini for 24 h. As expected, acini treated with control medium maintained acini-like structures and a clear lumen. On the contrary, all four macrophage-conditioned media (M1D, M1A, M2D and M2A) induced a dramatic increase in the

Downloaded from https://www.embopress.org on April 18, 2024 from IP 147.162.3.230.

 ª 2020 The Authors

percentage of acini with a partially or completely filled lumen (Figs 1B and C, and EV3D). Clearance of the lumen during the development of normal spheroids is the result of apoptosis following the detachment of cells from the extracellular matrix; thus, filling of the lumen can be the result of inhibition of cell death (Debnath & Brugge, 2005). However, we applied conditioned media at day 16, when the lumen had already been cleared and the cells were no longer proliferating; thus, we considered two other mechanisms to explain filling of the lumen, such as escape from proliferative arrest (Muthuswamy et al, 2001) and/or cell translocation in combination with acquisition of anchorage-independent survival properties (Leung & Brugge, 2012). To assess proliferation, we determined the expression of Ki67 (Scholzen & Gerdes, 2000) by immunofluorescence. The percentage of Ki67-positive cells was significantly increased in spheroids treated with M1D- and M1A-conditioned media, but not in M2D or M2A, indicating that M1 and M2 macrophages induce filling of the lumen via different mechanisms (Fig 1D and E). Since Rac activation has been implicated in anchorage-independent survival (Zahir et al, 2003), we took advantage of the Rac1 inhibitor NSC23766 (Gao et al, 2004) and tested its involvement in the macrophage-conditioned medium-induced filling of the lumen. Interestingly, Rac1 inhibition partially prevented this phenotype in

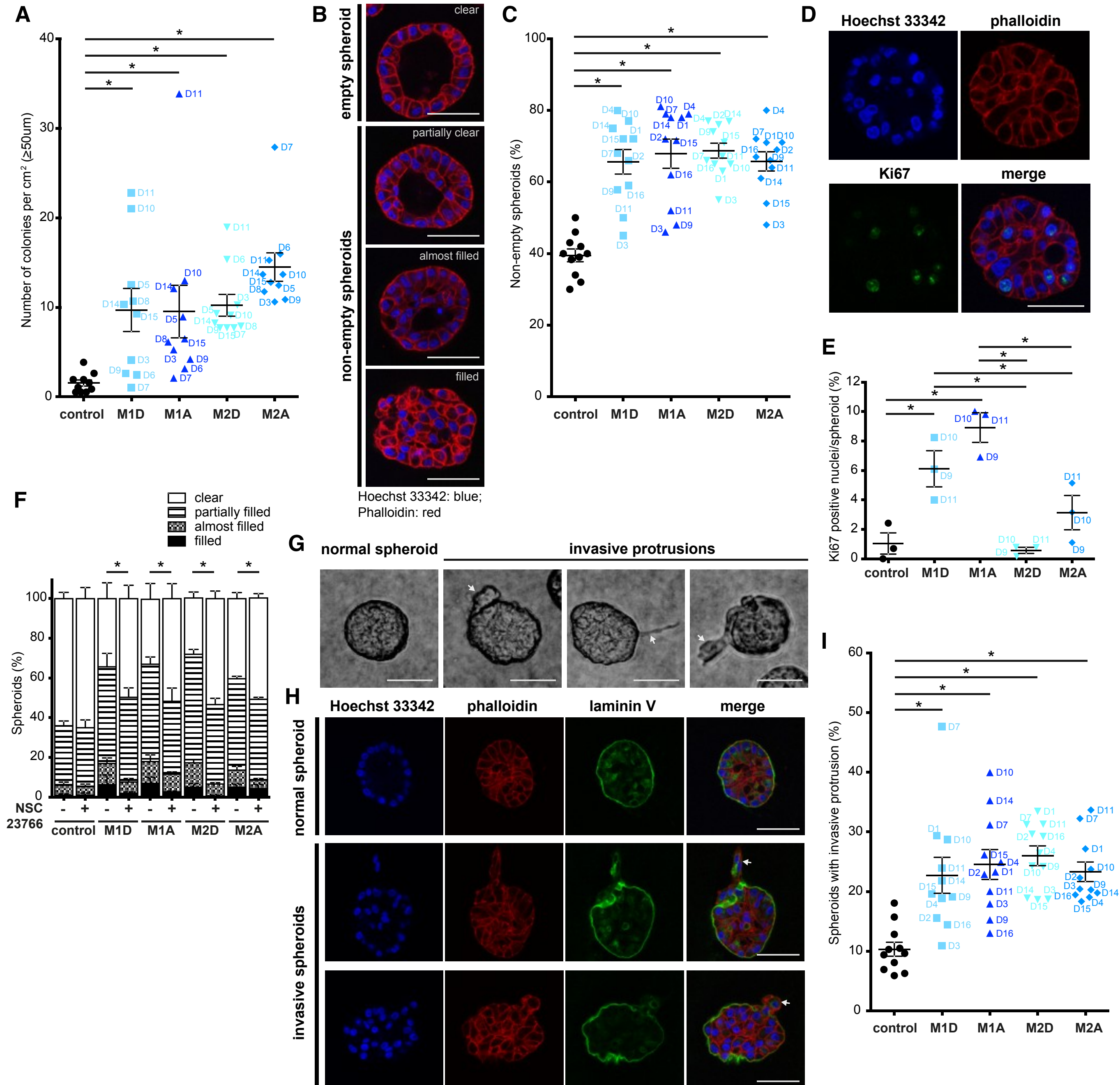

Figure 1.

Downloaded from https://www.embopress.org on April 18, 2024 from IP 147.162.3.230.

Figure 1. Macrophage-conditioned medium promotes anchorage-independent growth and invasiveness of MCF 10A cells.

Sixteen-day-old MCF10A spheroids grown in Matrigel/collagen mix were stimulated for 24 h with either macrophage-conditioned or control medium (B–I).

A Macrophage-conditioned medium induces MCF10A colony formation in soft agar as compared to control medium. Colonies ≥ 50 lm were counted at 5 weeks. Lines and error bars represent mean SEM from 10 independent experiments (n = 3 per condition). Data are shown also in Figs 4A and 6A.
B Representative images of MCF10A spheroids categorized into four groups according to the filling of the lumen with cell nuclei (clear, partially filled, almost filled and filled). Spheroids stained for DNA (Hoechst 33342 in blue) and F-actin (phalloidin in red).
C Macrophage-conditioned medium induces filling of the spheroid lumen with cell nuclei compared to control. Lines and error bars represent mean SEM from 11 independent experiments (n = 2 per condition, 50 spheroids each). Data are shown also in Figs 4D and 6D.
D Representative images of Ki67-positive nuclei of MCF10A cells. Spheroids stained for DNA (Hoechst 33342 in blue), F-actin (phalloidin in red) and Ki67 (green).
E Quantitative analysis of Ki67-positive nuclei per spheroid indicates enhanced proliferation of MCF10A cells upon stimulation with M1 macrophage-conditioned media. Lines and error bars represent mean SEM from three independent experiments (20–30 non-empty spheroids per condition).
F NSC23766 (Rac1 inhibitor; 50 lM) reduces the filling of the spheroid lumen with cell nuclei upon macrophage-conditioned medium stimulation compared to control. Filling of the spheroid lumen with cell nuclei categorized into four groups (clear, partially filled, almost filled and filled). Lines and error bars represent mean SEM from three independent experiments (n = 2 per condition, 50 spheroids each). Partially filled, almost filled and filled MCF10A spheroids were combined together (non-empty spheroids) for statistical analysis. All the data shown without the use of NSC23766 are also included in Fig EV3D.
G Invasive protrusions of spheroids into Matrigel/collagen mix marked with a white arrow.
H 3D structures of spheroids stained for DNA (Hoechst 33342 in blue), F-actin (phalloidin in red) and laminin V (green). Laminin V staining indicates the loss of basal membrane continuity at invasive protrusions. Invasive protrusions are marked with a white arrow.
I Macrophage-conditioned medium induces invasive protrusions in MCF10A spheroids compared to control. Lines and error bars represent mean SEM from 11 independent experiments (n = 2 per condition, at least 15 spheroids each from at least 2 fields of view). Data are shown also in Figs 4E and 6E.

Data information: Macrophage donors are indicated as D1–D16. M1D—M1-differentiated, M1A—M1-activated, M2D—M2-differentiated, M2A—M2-activated macrophages. *P < 0.05 as measured by one-way ANOVA with uncorrected Fisher's LSD post hoc test (exact P values are shown in Table EV2). Scale bar: 50 lm.
Source data are available online for this figure.

all conditions, indicating that this step is common in the signalling induced by both M1 and M2 macrophages (Figs 1F and EV3E).

Finally, we tested another Rac1-dependent process underlying malignant transformation, i.e. the formation of invasive protrusions accompanied by degradation of laminin V, previously reported in spheroids overexpressing HER2 and stimulated with tumour growth factor b (TGFb; Wang et al, 2006). Culturing 16-day-old MCF10A spheroids for 24 h in all four macrophage-conditioned media induced this invasive phenotype in agreement with Wolford et al (2013), typically resulting in one invasive protrusion per spheroid (Fig 1G–I). The effect was blocked by the Rac1 inhibitor NSC23766, as previously reported (Godinho et al, 2014) (Fig EV3F), with exception of M1A-conditioned medium. This phenotype was partially reproduced when testing MCF10A cell migration in 2D cultures, using a wound-healing assay. To exclude differential effects on cell proliferation, we performed this assay in the presence of mitomycin C. We showed that M1D-, M2D- and M2A-conditioned media induced a higher migration rate (wound confluency density ~80% versus ~60% of control medium at 48 h), while M1A-conditioned medium reduced the migration rate of MCF10A cells (wound confluency density around ~40% at 48 h; Fig EV3G and H).

Altogether, these data demonstrated that media conditioned by macrophages derived from healthy donors promote acquisition of fundamental malignant properties, such as anchorage-independent growth and invasiveness, in non-tumourigenic breast epithelial MCF10A cells grown in 3D. Of note, the strength of inducing different phenotypes varied between individual donors. For example, medium conditioned by D11-derived M1A induced the highest number of colonies in soft agar (Fig 1A), but had a weak effect in inducing invasive phenotype of the spheroids (Fig 1I).

Macrophage-conditioned medium induces malignant properties in primary mouse and human model systems

We then tested the effect of macrophage-conditioned media on mouse primary mammary organoids, a system that recapitulates main traits of the breast acini, where cells are organized in a bilayered structure of basal myoepithelial cells and internal luminal epithelial cells (Nguyen-Ngoc et al, 2015). Importantly, we confirmed formation of invasive protrusions in mouse primary organoids cultured in M1A- or M2A-conditioned medium (M1D and M2D were not tested on organoids) (Fig 2A and B). The staining for a-SMA revealed the loss of bilayered structure, with luminal cells found commonly at the front of invasive protrusions (Fig 2C). Macrophages infiltrate breast tissue early during obesity and are considered as inducing low level of chronic inflammation locally (Sun et al, 2012). Because this observation is recapitulated in a diet-induced model of obesity in mice (Arendt et al, 2013), we tested the invasive behaviour of mouse primary mammary organoids derived from animals on normal diet (ND) vs. high-fat diet (HFD) (Fig EV4A). As expected, animals on HFD were heavier than the ones on ND (average body weight: 27.2 1.48 g vs. 21.3 1.27 g, respectively), adipocytes in the mammary fat pad were on average larger (major adipocyte diameter: 74.4 17.1 lm vs. 42.5 7.7 lm), and we could observe a higher number of infiltrating macrophages (Fig EV4B–F), as previously reported (Subbaramaiah et al, 2011; Incio et al, 2018). When organoids were seeded in collagen, a substrate which promotes collective invasion (Nguyen-Ngoc et al, 2015), organoids derived from mice on HFD were more invasive than the ones derived from mice of ND (Fig 2D–F), suggesting that the environment created by HFD affects the invasive properties of the cells, via a mechanism that is conserved when the cells are cultured in vitro.

Altogether, these data demonstrated that media conditioned by macrophages derived from healthy donors promote acquisition of malignant properties in breast primary organoids. Moreover, HFD affects the invasive properties of these cells. Importantly, M1A- or M2A-conditioned medium also induced filling of the lumen—recapitulating ductal carcinoma in situ—in a recently established model where myoepithelial and luminal cells, isolated from reduction mammoplasty, are grown in collagen and reform into bilayer structures (Fig 2G and H), a phenotype induced also by overexpression of HER2 (Carter et al, 2017).

Downloaded from https://www.embopress.org on April 18, 2024 from IP 147.162.3.230.

ª 2020 The Authors

IKKe expression is associated with tumour inflammation and mediates the macrophage-conditioned medium-induced malignant phenotype

The breast cancer oncogene IKKe is a kinase linking obesity and inflammation, and inflammation and cancer (Olefsky, 2009); thus, we tested its role in inflammation-mediated transformation of breast epithelial cells. First, to test the association between IKKe expression and tumour inflammation, we performed semi-quantitative analysis of IKKe expression and immune cell infiltration by immunohistochemistry in a cohort of 66 human breast cancers (Table EV2). We observed that in 83% of cases, the kinase was expressed at medium or high level (Fig 3A and B), which showed strong correlation with the inflammatory grade (Spearman's correlation coefficient 0.619, P < 0.0001) (Figs 3C and EV5A). Interestingly, the level of expression of IKKe was distributed heterogeneously in tumours, with higher expression in small tumour cell patches in the stroma and at the invasive front (Fig EV5B and C). Moreover, transcriptomic analysis of the METABRIC breast cancer dataset (Curtis et al, 2012) confirmed that the transcript levels of IKBKE mRNA and the immune infiltration-associated gene expression pattern (immune score, ESTIMATE; Yoshihara et al, 2013) are correlated (Fig 3D), while the IKBKE gene was amplified only in a few cases (Fig 3E). Importantly, the expression of TBK1 showed no correlation with the immune score (Fig EV5D), indicating the specific involvement of IKKe in the response.

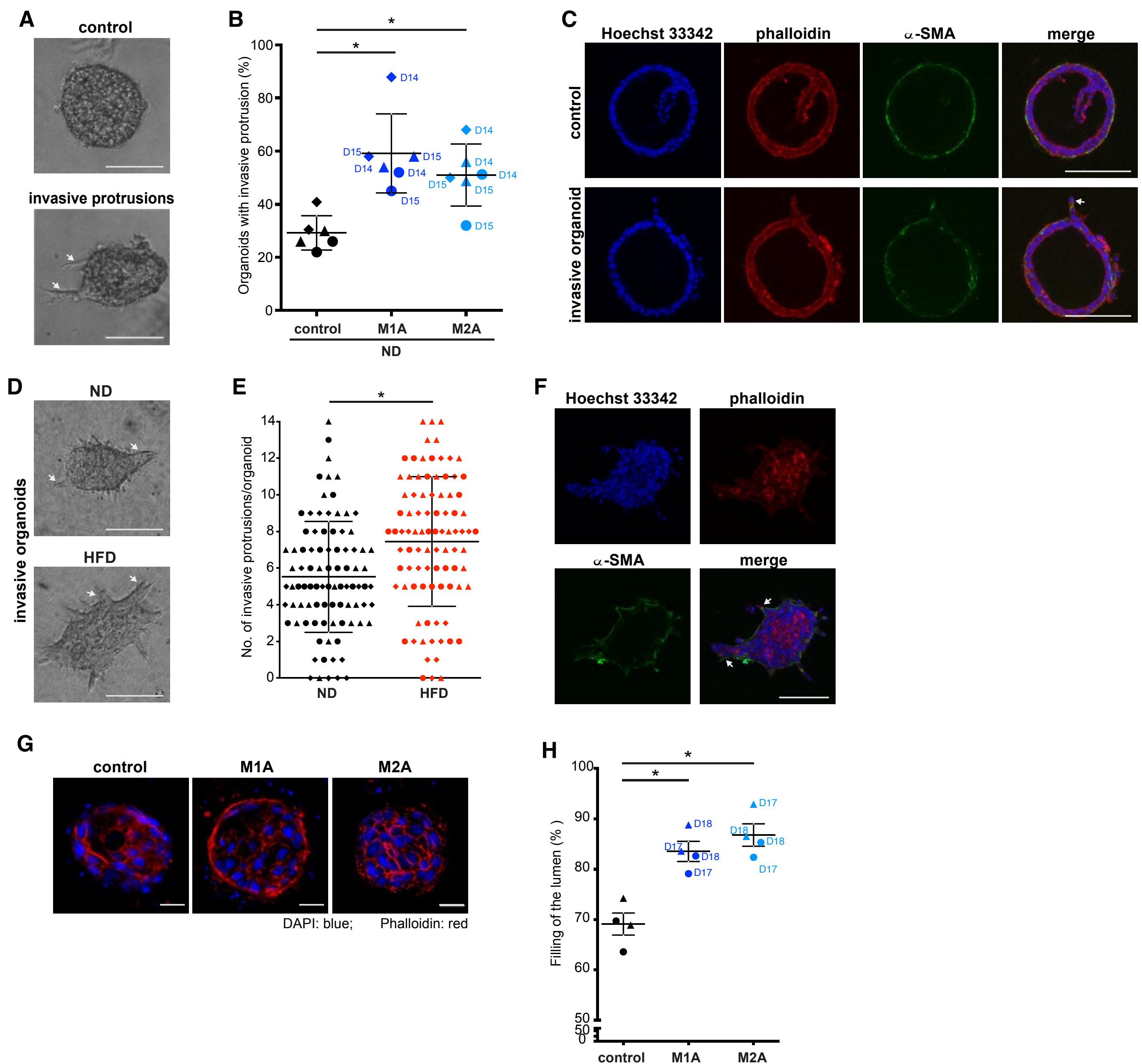

Figure 2.

Downloaded from https://www.embopress.org on April 18, 2024 from IP 147.162.3.230.

Figure 2. Macrophage-conditioned medium promotes acquisition of malignant properties in mouse mammary organoids and human ductal structures.

Mammary organoids were isolated from 19- to 20-week-old C57Bl/6 mice on normal (ND) or high-fat diet (HFD) (n = 3) (A–F).

A–C Organoids isolated from ND mice were cultured in Matrigel/collagen mix for 2 days followed by macrophage-conditioned or control medium stimulation for 24 h. (A) Representative images of organoids in Matrigel/collagen mix. (B) Macrophage-conditioned medium induces invasive protrusions in organoids as compared to control. Lines and error bars represent mean SEM from three independent experiments, with each mouse labelled with a different symbol shape (n = 2 per condition; 15–25 organoids each). *P < 0.05 as measured by one-way ANOVA with uncorrected Fisher's LSD post hoc test. Data are shown also in Figs 4F and 6F. (C) 3D structure of organoids stained for DNA (Hoechst 33342 in blue), F-actin (phalloidin in red) and a-SMA (green). Bilayered structure of internal luminal cells and external basal myoepithelial cells is established for non-invasive organoids.

D–F Organoids isolated from ND or HFD mice were cultured in collagen for 2 days. (D) Representative images of organoids cultured in collagen for 2 days. (E) The number of invasive protrusions per organoid is higher for organoids isolated from mice on HFD compared to mice on ND. Lines and error bars represent mean SD from three independent experiments where 30 organoids were counted per each mouse (labelled with a different symbol shape). *P < 0.05 as measured by two-tailed Student's t-test. Data are shown also in Figs 4G/H and 6G/H. (F) 3D structure of organoid stained for DNA (Hoechst 33342 in blue), F-actin (phalloidin in red) and a-SMA (green). a-SMA, myoepithelial cell marker, appeared to be loss at invasive protrusions.

G,H Human myoepithelial and luminal cells isolated from breast specimens were cultured in collagen gels for 14 days to reform ductal structures with luminal compartment. Reformed ducts were then cultured for 7 days in macrophage-conditioned or control medium. (G) Representative images of ductal structures cultured with conditioned medium. Ducts were stained for DNA (DAPI in blue) and F-actin (phalloidin in red). (H) Macrophage-conditioned medium induces filling of the duct lumen with cell nuclei compared to control. Lines and error bars represent mean SEM (a total of 24 structures were counted per each condition: 2 patient ductal structures (n = 2), each labelled with a different symbol shape, were cultured with macrophage-conditioned media from either donor 17 or donor 18, 3 ducts each). Filling of the lumen was determined as % of luminal space filled with cells. *P < 0.05 as measured by one-way ANOVA with uncorrected Fisher's LSD post hoc test.

Data information: Macrophage donors are indicated as D10, D15, D17, D18. M1A—M1-activated, M2A—M2-activated macrophages. Data are shown also in Figs 4J and 6J. Exact P values are shown in Table EV3. Invasive protrusions are marked with a white arrow. Scale bar: 100 lm (A, C, D, F) or 20 lm (G).
Source data are available online for this figure.

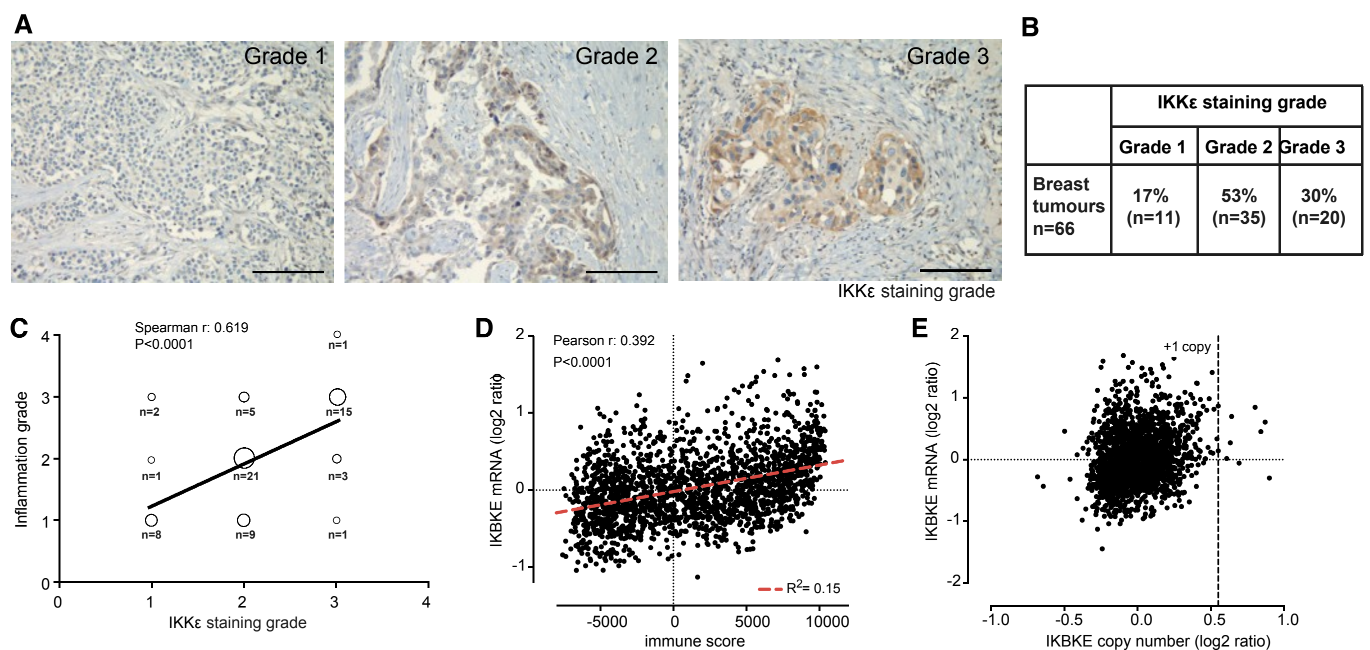

Figure 3. IKKe expression in breast cancer is associated with immune infiltration.

A IKKe expression was assessed semi-quantitatively using a 0–3 grade scale ("0": no staining; "1": weak; "2": moderate; "3": strong) on human breast cancer sections using immunohistochemistry. Representative images according to the IKKe staining grade are shown. Scale bar: 100 lm.

B Distribution table of IKKe expression in the cohort of 66 human breast carcinomas according to the staining grade.

C Correlation between IKKe expression and immune cell infiltration ("0": no inflammatory cells; "1": weak; "2": moderate; "3": strong; "4": very strong). Bubble plot of IKKe and immune infiltration grades, size shows the number of tumours falling in the category. Spearman's rho coefficient and significance of difference from slope = 0 (P) are shown.

D Correlation between IKBKE mRNA levels (log2 ratio) and immune signature (Yoshihara et al, 2013) in the METABRIC transcriptomic dataset from 1981 breast cancer patients (Curtis et al, 2012). Pearson's correlation rho coefficient and significance of difference from slope = 0 (P) are shown.

E IKBKE gene copy number and mRNA levels (log2 ratio) from the METABRIC transcriptomic dataset (see D) are plotted. Estimated + 1 copy number values are shown by the dotted vertical line. No significant correlation by Pearson's correlation rho coefficient and significance of difference from slope = 0 (P) was detected.

Source data are available online for this figure.

ª 2020 The Authors

Downloaded from https://www.embopress.org on April 18, 2024 from IP 147.162.3.230.

To demonstrate the functional role of IKKe in the macrophage-mediated transformation, we then used the recently identified inhibitor of IKKe/TBK1, amlexanox, an FDA-approved drug previously used for the treatment of mouth ulcers (Reilly et al, 2013). Strikingly, when amlexanox 50 lM (as used in ref. Reilly et al, 2013) was added to macrophage-conditioned media applied to MCF10A cells, we observed strong inhibition of all cellular transformation-related features, such as anchorage-independent growth (Fig 4A), filling of the spheroid lumen (Fig 4B–D) and formation of invasive protrusions (Fig 4E) induced by M1D-, M1A-, M2A- and M2D-conditioned media. Moreover, amlexanox reduced the percentage of organoids with invasive protrusions induced by M1A- and M2A-conditioned media in mouse primary breast organoids (Fig 4F) as well as the number of invasive protrusions observed in organoids derived from animals on ND and HFD (Fig 4G and H). Filling of the lumen was inhibited by amlexanox also in the human model system where myoepithelial and luminal cells, isolated from reduction mammoplasty, are grown in collagen and reform into bilayer structures (Fig 4I and J). Confirming the crucial role played by IKKe in the phenotypes induced by macrophage-conditioned media, MCF10A cells where the IKBKE gene (encoding for IKKe) has been deleted via CRISPR/Cas9 formed dramatically less colonies in soft agar and failed to form invasive protrusions (Figs 4K and L, and EV6A and B).

The effect of amlexanox also in control conditions, both in MCF10A and in organoids, suggests a basal level of IKKe activity.

Altogether, these data indicate that expression of IKKe at the very early stages of transformation is associated with inflammation and amlexanox inhibits acquisition of malignant properties induced by macrophage-conditioned medium.

NCT502, an inhibitor of PHGDH, prevents macrophage-conditioned medium-induced malignant phenotype

We have recently observed that IKKe regulates the serine biosynthesis pathway (SBP) (https://biorxiv.org/cgi/content/short/855361v1), which previously was reported to support tumour formation and growth via multiple mechanisms (Locasale, 2013). Phosphoglycerate dehydrogenase (PHGDH), the first enzyme of the pathway, is an established oncogene in breast cancer and melanoma (Locasale et al, 2011; Possemato et al, 2011), and when overexpressed in MCF10A spheroids, it leads to the formation of disorganized spheroids with filled lumen (Locasale et al, 2011). To assess whether this pathway is associated with the inflammatory phenotype in breast cancer, we first analysed the level of expression of phosphoserine aminotransferase 1 (PSAT1, second enzyme of the serine biosynthesis pathway) that we recently observed to be regulated by IKKe (https://biorxiv.org/cgi/content/short/855361v1). We

Figure 4. The macrophage-mediated transforming effect is reduced by amlexanox, an inhibitor of IKKe/TBK1, or upon IKKe deletion.

A Amlexanox inhibits colony formation of MCF10A cells grown in soft agar with macrophage-conditioned medium for 5 weeks compared to controls. Colonies ≥ 50 lm were counted. Lines and error bars represent mean SEM from 10 independent experiments (n = 3 per condition). All the data shown without the use of amlexanox are also included in Fig 1A.

B–E Sixteen-day-old MCF10A spheroids grown in Matrigel/collagen mix were stimulated for 24 h with either macrophage-conditioned or control medium in the presence of amlexanox. (B) Representative images showing the filling of the spheroid lumen with cell nuclei. The spheroids were stained for DNA (Hoechst 33342 in blue) and F-actin (phalloidin in red). Scale bar: 50 lm. (C,D) Amlexanox reduces filling of the spheroid lumen with cell nuclei. (C) Filling of the spheroid lumen with cell nuclei categorized into 4 groups (clear, partially filled, almost filled and filled). (D) Filling of the spheroid lumen with cell nuclei. Partially filled, almost filled and filled spheroids were combined together (non-empty spheroids). Lines and error bars represent mean SEM from seven independent experiments (n = 2 per condition; 50 spheroids each). Partially filled, almost filled and filled spheroids were combined together (non-empty spheroids) for statistical analysis. All the data shown without the use of amlexanox are also included in Figs EV3D and 1C, respectively. (E) Amlexanox reduces the number of spheroids with invasive protrusions. Lines and error bars represent mean SEM from eight independent experiments (n = 2 per condition, at least 15 spheroids each from at least 2 fields of view). All the data shown without the use of amlexanox are also included in Fig 1I.

F–H Mammary organoids were isolated from 19- to 20-week-old C57Bl/6 mice on normal (ND) or high-fat diet (HFD) (n = 3). (F) Organoids isolated from mice on ND were cultured in Matrigel/collagen mix for 2 days and then stimulated with macrophage-conditioned or control medium in the presence of amlexanox. Amlexanox reduces the number of invasive organoids. Lines and error bars represent mean SEM from three independent experiments, with each mouse labelled with a different symbol shape (n = 2 per condition; 15–25 organoids each). All the data shown without the use of amlexanox are also included in Fig 2B. (G,H) Organoids were cultured in collagen for 2 days after which the number of invasive protrusions per each organoid was determined microscopically. Amlexanox reduces the number of invasive protrusions in organoids isolated from mice on (G) ND or (H) HFD. Lines and error bars represent mean SD from 3 independent experiments where 30 organoids were counted per each mouse (labelled with a different symbol shape). All the data shown without the use of amlexanox are also included in Fig 2E.

I, J Human myoepithelial and luminal cells isolated from breast specimens were cultured in collagen gels for 14 days to reform ductal structures with luminal compartment. Reformed ducts were then cultured for 7 days in macrophage-conditioned or control medium in the presence of amlexanox. (I) Representative images showing the filling of the ductal lumen with cell nuclei. The ducts were stained for DNA (DAPI in blue) and F-actin (phalloidin in red). Scale bar: 20 lm. (J) Amlexanox inhibits filling of the duct lumen with cell nuclei. Lines and error bars represent mean SEM (a total of 24 structures were counted per each condition: 2 patient ductal structures (n = 2), each labelled with a different symbol shape, were cultured with macrophage-conditioned media from either donor 17 or donor 18, 3 ducts each). Filling of the lumen was determined as % of luminal space filled with cells. All the data shown without the use of amlexanox are also included in Fig 2H.

K, L IKBKE gene (encoding for IKKe) was deleted in MCF10A cells via CRISPR-Cas9 technology. Three knockout clones were combined for each cell line. (K) IKKe CRISPR-Cas9 knockout MCF10A cells form less colonies when grown in soft agar with macrophage-conditioned medium for 5 weeks compared to CRISPR-Cas9 control (non-targeting crRNA) cells. Colonies ≥ 50 lm were counted. (L) Sixteen-day-old MCF10A spheroids grown in Matrigel/collagen mix were stimulated for 24 h with either macrophage-conditioned or control medium. IKKe CRISPR-Cas9 knockout MCF10A cells are less invasive compared to CRISPR control (non-targeting crRNA) cells. Lines and error bars represent mean SEM from 3 independent experiments (n = 3 per condition). Media from two macrophage donors were combined in 1:1 ratio in each experiment.

Data information: Macrophage donors are indicated as D1-D25. M1D—M1-differentiated, M1A—M1-activated, M2D—M2-differentiated, M2A—M2-activated macrophages. Aml.—amlexanox (50 lM). *$P < 0.05$ as measured by two-tailed Student's t-test (exact P values are shown in Table EV3).
Source data are available online for this figure.

Downloaded from https://www.embopress.org on April 18, 2024 from IP 147.162.3.230.

ª 2020 The Authors

Downloaded from https://www.embopress.org on April 18, 2024 from IP 147.162.3.230.

Figure 4.

ª 2020 The Authors

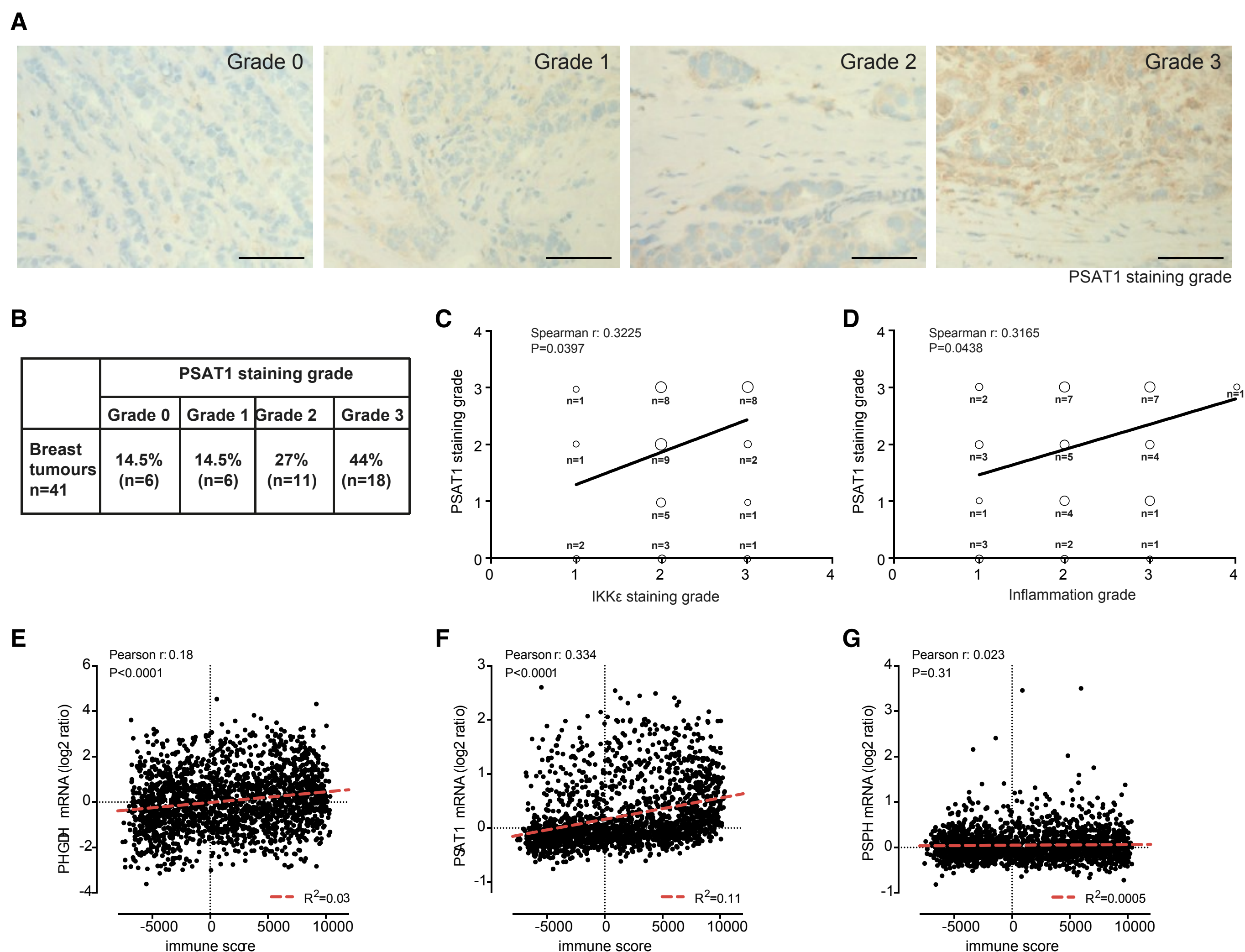

	PSAT1 staining grade			
	Grade 0	Grade 1	Grade 2	Grade 3
Breast tumours n=41	14.5% (n=6)	14.5% (n=6)	27% (n=11)	44% (n=18)

Figure 5. PSAT1 expression in breast cancer is associated with IKKe expression and immune infiltration.

A PSAT1 expression was assessed semi-quantitatively using a 0-3 grade scale (“0”: no staining; “1”: weak; “2”: moderate; “3”: strong) on human breast cancer sections using immunohistochemistry. Representative images according to the PSAT1 staining grade are shown. Scale bar: 50 lm.

B Distribution table of PSAT1 expression in the cohort of 41 human breast carcinomas according to the staining grade.

C Correlation between PSAT1 and IKKe expression (“0”: no staining; “1”: weak; “2”: moderate; “3”: strong). Bubble plot of PSAT1 and IKKe staining grades, size shows the number of tumours falling in the category.

D Correlation between PSAT1 and immune cell infiltration (“0”: no inflammatory cells; “1”: weak; “2”: moderate; “3”: strong; “4”: very strong). Bubble plot of PSAT1 and immune infiltration grades, size shows the number of tumours falling in the category.

E–G Correlation of mRNA levels of the SBP enzyme genes PSAT1 (E), PHGDH (F), PSPH (G) with the immune signature (Yoshihara et al, 2013) in the METABRIC transcriptomic dataset from 1981 breast cancer patient (Curtis et al, 2012).

Data information: Spearman’s (C, D) or Pearson’s (E–G) correlation rho coefficient and significance of difference from slope = 0 (P) are shown.
Source data are available online for this figure.

used frozen sections of 41 patients of the cohort previously used for IKKe staining to semi-quantitatively define PSAT1 expression. We found that in 71% of cases, the protein was expressed at medium or high level (grade 2 or 3, Fig 5A and B). Importantly, we found a significant correlation of PSAT1 expression with IKKe levels and the inflammatory grade of the same samples (Fig 5C and D), indicating association between inflammation and SBP in breast tumours.

We also found significant correlation between the transcript levels of two out of three SBP enzymes—PHGDH and PSAT1—and the immune infiltration-associated gene expression pattern (immune score, ESTIMATE) (Yoshihara et al, 2013) (Fig 5E–G) in the METABRIC breast cancer transcriptome dataset (Curtis et al, 2012), indicating that inflammation is also a key regulator of the SBP in addition to known oncogenes (Yang & Vousden, 2016).

These results suggested that activation of the SBP downstream of IKKe could contribute to the acquisition of malignant properties in MCF10A cells induced by macrophage-conditioned medium. To test this hypothesis, we applied NCT502 (10 lM), a recently

Downloaded from https://www.embopress.org on April 18, 2024 from IP 147.162.3.230.

developed inhibitor of PHGDH (Pacold et al, 2016), to the macrophage-conditioned media. Similarly to the effect of IKKe inhibition by amlexanox, NCT502 prevented anchorage-independent growth (Fig 6A) and filling of the lumen (Fig 6B–D) induced by M1D-, M1A-, M2A- and M2D-conditioned media. NCT502 also inhibited formation of invasive protrusions induced by M1D, M2A and M2D, but not by M1A (Fig 6E). Furthermore, NCT502 reduced the percentage of organoids with invasive protrusions induced by M1A- and M2A-conditioned media in primary mouse breast organoids (Fig 6F) and reduced the number of invasive protrusions in organoids derived from animals on ND and HFD (Fig 6G and H). Importantly, filling of the spheroid lumen was inhibited by NCT502 also in the human model system where bilayer structures are formed in collagen by myoepithelial and luminal cells isolated from reduction mammoplasty (Fig 6I and J). Confirming the crucial role played by the SBP downstream of IKKe, macrophage-conditioned media did not induce any phenotype (i.e. colonies in soft agar and invasive protrusions) in MCF10A cells where the PHGDH gene has been deleted via CRISPR/Cas9 (Figs 6K and L, and EV6A and B).

These data indicate that activation of the SBP is essential for the acquisition of the malignant phenotypes induced by macrophage-conditioned media.

Amlexanox delays tumourigenesis in vivo in a genetic breast cancer mouse model combined with diet-induced obesity

It has been previously shown that HFD-induced obesity enhances mammary carcinogenesis in a mouse model of breast cancer carrying a heterozygous copy of the mouse mammary tumour virus–polyomavirus middle T antigen (MMTV-PyMT) (Cowen et al, 2015). Thus, we used this model to test whether IKKe plays a role in obesity-induced tumourigenesis.

Six- to seven-week-old female mice (MMTV-PyMT$^{+/}$, 10 per group) were fed on ND or HFD, and a week after the start of the diet, they received vehicle or amlexanox treatment by daily oral gavage (Fig 7A). A smaller cohort of WT animals were kept on the same diet to control for possible unpredicted effects of the MMTV-PyMT gene. Body weight and tumour appearance were monitored for a total period of 12 weeks (from the first week after beginning of the diet). Wild-type mice on HFD gained significantly more weight (Fig 7B), adipocytes were larger in the mammary fat pad (Fig 7C), and more infiltrating macrophages were observed (Fig 7D). MMTV-PyMT$^{+/}$ animals also gained more weight on the HFD regime, which was unaffected by amlexanox treatment (Fig 7E–G), differently from what previously reported (Reilly et al, 2013). Importantly, however, tumour latency was significantly

Figure 6. The macrophage-mediated transforming effect is reduced by NCT502, PHGDH inhibitor or upon PHGDH deletion.

A NCT502 (10 lM) inhibits colony formation of MCF10A cells grown in soft agar with macrophage-conditioned medium for 5 weeks compared to controls. Colonies ≥ 50 lm were counted. Lines and error bars represent mean SEM from five independent experiments (n = 3 per condition). All the data shown without the use of NCT502 are also included in Fig 1A.

B–E Sixteen-day-old MCF10A spheroids grown in Matrigel/collagen mix were stimulated for 24 h with either macrophage-conditioned or control medium in the presence of NCT502 (10 lM). (B) Representative images showing the filling of the spheroid lumen with cell nuclei. The spheroids were stained for DNA (Hoechst 33342 in blue) and F-actin (phalloidin in red). Scale bar: 50 lm. (C, D) NCT502 reduces the filling of the spheroid lumen with cell nuclei. (C) Filling of the spheroid lumen with cell nuclei categorized into 4 groups (clear, partially filled, almost filled and filled). (D) Filling of the spheroid lumen with cell nuclei. Partially filled, almost filled and filled spheroids were combined together (non-empty spheroids). Lines and error bars represent mean SEM from 3 independent experiments (n = 2 per condition; 50 spheroids each). Partially filled, almost filled and filled spheroids were combined together (non-empty spheroids) for statistical analysis. All the data shown without the use of NCT502 are also included in Figs EV3D and 1C, respectively. (E) NCT502 reduces the number of spheroids with invasive protrusions (n = 2 per condition). Lines and error bars represent mean SEM from three independent experiments (n = 2 per condition; at least 15 spheroids each from at least 2 fields of view). All the data shown without the use of NCT502 are also included in Fig 1I.

F–H Mouse mammary organoids were isolated from 19- to 20-week-old C57Bl/6 mice that were either on normal (ND) or high-fat diet (HFD) (n = 3). (F) Organoids were isolated from mice on ND and cultured in Matrigel/collagen mix for 2 days followed by macrophage-conditioned or control medium stimulation for 24 h in the presence of NCT502 (10 lM). NCT502 reduces the number of invasive organoids. Lines and error bars represent mean SEM from 3 independent experiments, with each mouse labelled with a different symbol shape (n = 2 per condition; 15–25 organoids each). All the data shown without the use of NCT502 are also included in Fig 2B. (G,H) Organoids were cultured in collagen for 2 days after which the number of invasive protrusions per each organoid was determined microscopically. NCT502 (10 lM) reduces the number of invasive protrusions in organoids isolated from mice that were either on (G) ND or (H) HFD. Lines and error bars represent mean SD from 3 independent experiments where 30 organoids were counted per each mouse (labelled with a different symbol shape). All the data shown without the use of NCT502 are also included in Fig 2E.

I, J Human myoepithelial and luminal cells isolated from breast specimens were cultured in collagen gels for 14 days to reform ductal structures with luminal compartment. Reformed ducts were then cultured for 7 days in macrophage-conditioned or control medium in the presence of NCT502 (10 lM). (I) Representative images showing the filling of the ductal lumen with cell nuclei. The ducts were stained for DNA (DAPI in blue) and F-actin (phalloidin in red). Scale bar 20 lm. (J) NCT502 inhibits filling of the duct lumen with cell nuclei. Lines and error bars represent mean SEM (a total of 24 structures were counted per each condition: 2 patient ductal structures (n = 2), each labelled with a different symbol shape, were cultured with macrophage-conditioned media from either donor 17 or donor 18, 3 ducts each). Filling of the lumen was determined as % of luminal space filled with cells. All the data shown without the use of NCT502 are also included in Fig 2H.

K, L PHGDH gene was deleted in MCF10A cells via CRISPR-Cas9 technology. Three knockout clones were combined for each cell line. (K) PHGDH CRISPR-Cas9 knockout MCF10A cells form less colonies when grown in soft agar with macrophage-conditioned medium for 5 weeks compared to CRISPR-Cas9 control (non-targeting crRNA) cells. Colonies ≥ 50 lm were counted. (L) Sixteen-day-old MCF10A spheroids grown in Matrigel/collagen mix were stimulated for 24 h with either macrophage-conditioned or control medium. PHGDH CRISPR-Cas9 knockout MCF10A cells are less invasive compared to CRISPR control (non-targeting crRNA) cells. Lines and error bars represent mean SEM from 3 independent experiments (n = 3 per condition). Media from two macrophage donors were combined in 1:1 ratio in each experiment.

Data information: Macrophage donors are indicated as D1-D25. M1D—M1-differentiated, M1A—M1-activated, M2D—M2-differentiated, M2A—M2-activated macrophages. *$P < 0.05$ as measured by two-tailed Student's t-test (exact P values are shown in Table EV3).
Source data are available online for this figure.

Downloaded from https://www.embopress.org on April 18, 2024 from IP 147.162.3.230.

ª 2020 The Authors

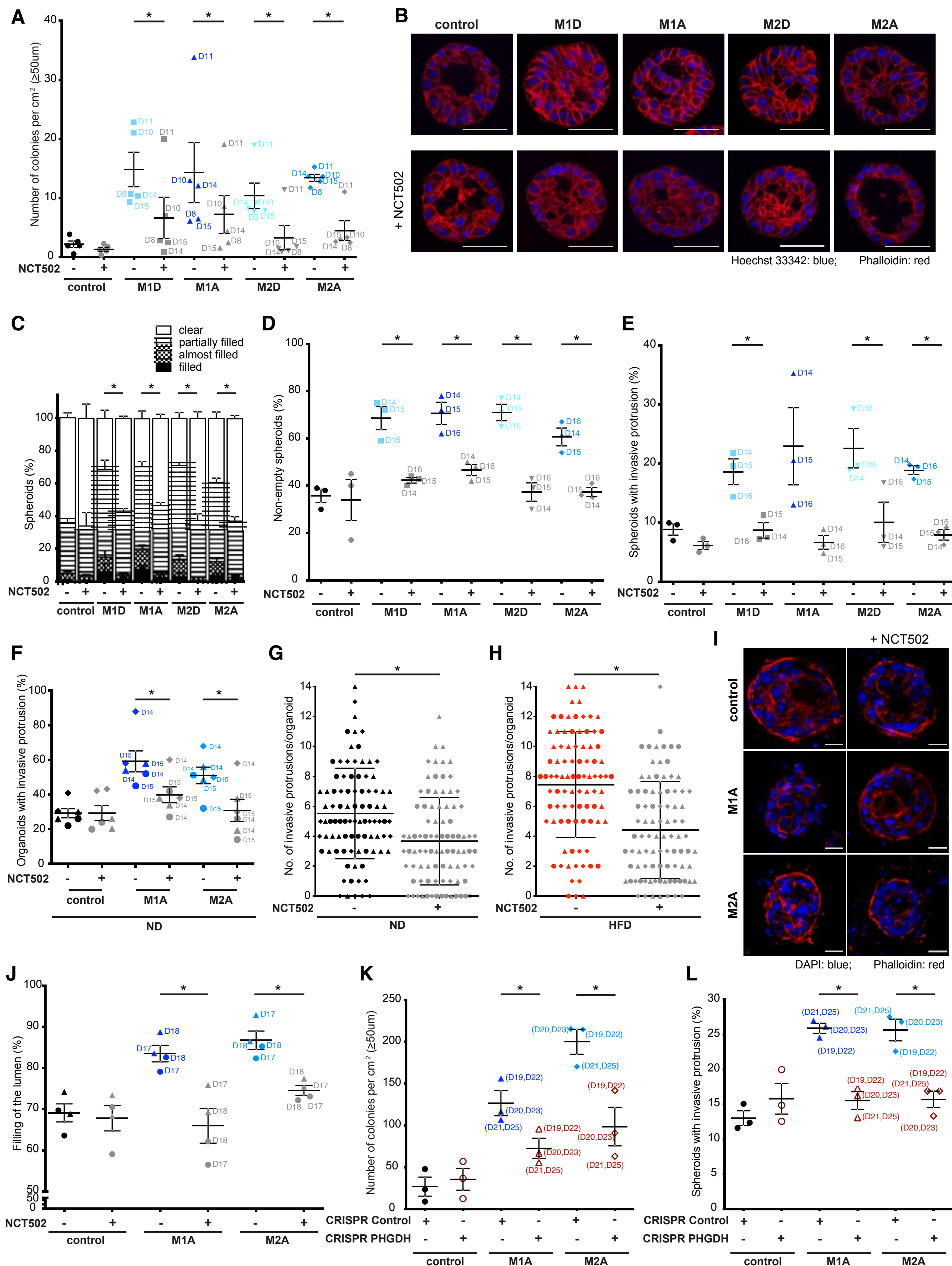

Figure 6.

Downloaded from https://www.embopress.org on April 18, 2024 from IP 147.162.3.230.

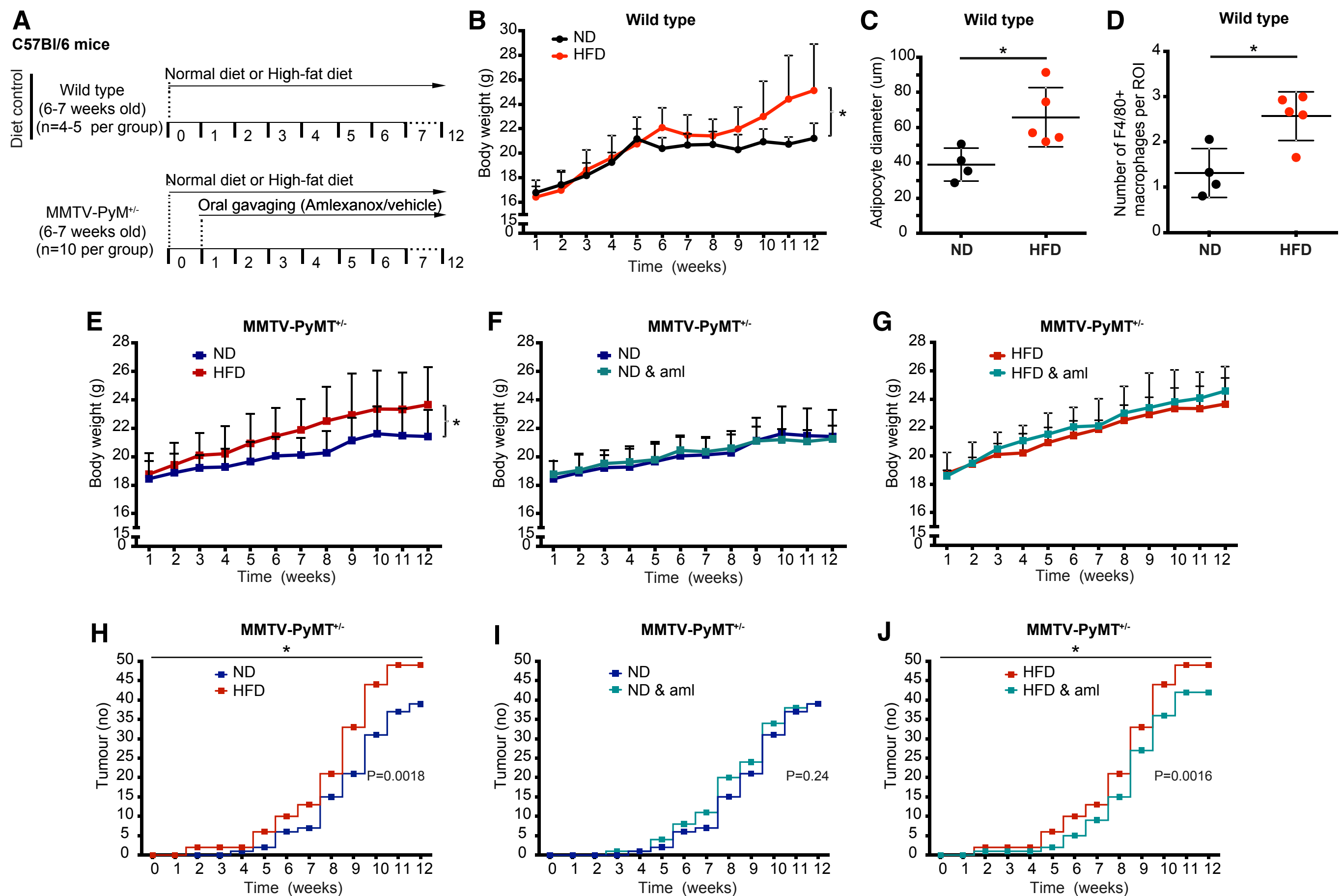

Figure 7. Amlexanox delays tumour formation in a diet-induced obesity/PyMT-MMTV mouse model.

Ten per group female C57Bl/6 mice heterozygous for the PyMT-MMTV started high-fat diet (HFD) when 6- to 7-week-old (prior of mammary tumour development) together with control mice on normal diet (ND; n = 10). Mice were administered amlexanox (17 mM) or vehicle control daily by oral gavage (Reilly et al, 2013).A control group (wild-type mice) was also included to confirm the efficacy of the diet and to control for possible unpredicted interactions of the MMTV-PyMT gene.

- A Schematic representation of combined genetic mouse model of breast cancer and high-fat diet-induced obesity used to study the effects of amlexanox in tumour formation.
- B Wild-type mice on HFD gain more weight compared to ND mice. *$P < 0.05$ by one-tailed Student's t-test.
- C Average adipocytes size (major diameter) in mammary fat pads is larger in HFD mice compared to ND mice based on the analysis of at least 100 adipocytes per mice on H&E-stained sections. *$P < 0.05$ by two-tailed Student's t-test.
- D The number of F4/80 + macrophages in mammary fat pads is increased in HFD mice compared to ND mice. The average of F4/80 + macrophages in at least 10 fields of view per mouse is shown. *$P < 0.05$ by two-tailed Student's t-test.
- E PyMT-MMTV+/- mice on HFD gain more weight compared to ND mice. *$P < 0.05$ by one-tailed Student's t-test.
- F,G Amlexanox does not affect weight gain either in mice on F) ND or G) HFD.
- H Mammary tumours are developing earlier in PyMT-MMTV+/- mice on HFD compared to ND mice. P value was calculated using log-rank test.
- I, J Amlexanox does not affect tumour development in PyMT-MMTV+/- mice on (I) ND, but delays tumour formation in (J) HFD mice. P value was calculated using log-rank test.

Data information: Lines and error bars represent mean and SD. Exact P values are shown in Table EV3.
Source data are available online for this figure.

decreased by HFD (Fig 7H), and while no effect of amlexanox was observed on tumour appearance in mice on ND (Fig 7I), the effect of HFD was significantly reverted by amlexanox treatment (Fig 7J).

These data showed that diet-induced obesity synergizes with MMTV-PyMT in promoting tumour formation and inhibition of IKKe/TBK1 by amlexanox delays tumour appearance in mice on HFD, even when induced by a strong oncogene, such a PyMT.

Discussion

Obesity is estimated to be the cause of cancer in 14% of cases in men and around 20% in women (Calle et al, 2003). Despite many indications that a critical factor increasing the risk of cancer in obese patients is obesity-associated inflammation, partially caused by infiltrating macrophages, little is known about the mechanism(s) underlying this phenomenon. While macrophages were shown to play a

Downloaded from https://www.embopress.org on April 18, 2024 from IP 147.162.3.230.

ª 2020 The Authors

crucial role at different stages of cancer progression (Williams et al, 2016), here we studied their role in promoting the very early stages of malignant transformation, using macrophage-conditioned medium derived from 25 healthy donors.

We report that macrophages induce acquisition of malignant phenotypes in three independent model systems: (i) the non-tumourigenic MCF10A cell line, (ii) mouse primary organoids and (iii) human primary breast epithelial cells derived from patients. We also further show that acquisition of malignant properties induced by macrophage-conditioned medium can be prevented by genetic (via CRISPR/Cas9) inhibition of IKKe and PHGDH and pharmacologically, via amlexanox, a recently identified inhibitor of IKKe/TBK1, and NCT502, an inhibitor of PHGDH. Moreover, amlexanox delayed tumour appearance in vivo in a combined diet-induced obesity/ MMTV-PyMT breast cancer model.

Amlexanox is an FDA-approved drug for the treatment of aphthous ulcers, rediscovered as IKKe/TBK1 inhibitor, that in mice improves obesity-related metabolic dysfunction (Reilly et al, 2013), suggesting that it targets processes linking inflammation to metabolism. Recently, the drug has been tested in a proof-of-concept study in obese patients with type 2 diabetes and non-alcoholic fatty liver disease, where it improved metabolic parameters in a subset of patients characterized by a specific inflammatory signature in subcutaneous fat. Importantly, the safety of the use of amlexanox in humans was confirmed, with the only side effect reported being rash, in the majority of the cases classified as non-clinically relevant (Oral et al, 2017). The level of inflammation in the white adipose tissue is considered an important factor distinguishing metabolically unhealthy obese patients from metabolically healthy ones and is also a characteristic of 20% of the metabolically unhealthy lean population (Stefan et al, 2017). Thus, in the context of a potential clinical follow-up of our study, the level of inflammation in the breast of obese patients should be a key parameter to be used for stratifying patients and to increase the probability of a successful preventive effect. Importantly, in humans, as in our study, amlexanox did not cause a significant reduction in body weight, suggesting that its most likely mechanism of action is a direct preventive effect of inflammation, and not an event secondary to the effect on whole-body metabolism.

The other compound we tested, the PHGDH inhibitor NCT502, shows efficacy in vivo to reduce growth of tumours overexpressing PHGDH (Pacold et al, 2016). Here, we report a possible preventive role for this molecule in obese patients with signs of inflammation, also highlighting a new regulatory mechanism for SBP.

An unexpected finding of our study is that media conditioned by the four macrophage populations, independently of the activation state, led to acquisition of malignant characteristics. The fact that differentiated macrophages, before activation, induce the malignant phenotype can be explained by their secretory activity (Fig EV1C–J and Table EV1). Moreover, while the four different conditioned media induce a similar malignant phenotype, it is important to highlight that from a mechanistic point of view M1 and M2, macrophages use different strategies, with M1 (differentiated or activated), but not M2, being able to overcome the proliferative arrest in MCF10A spheroids. Thus, while a common factor might be secreted by the four cell types (Jablonski et al, 2015), another possible scenario is that the same phenotype is achieved by different signalling pathways, activated by different cytokines.

Importantly, we found that the expression of CD206 is characteristic of the M1D and M2A populations (Fig EV2E and G). Recently, macrophages present in the breast of obese women were shown to express the same marker and to resemble more M2 than M1 subtype, bearing also similarities to tumour-associated macrophages (Springer et al, 2019). Macrophages in the breast have also been reported to reprogramme during obesity, become metabolically activated and different from M1 macrophages due to their pro-tumourigenic activity (Tiwari et al, 2019). However, since the extent of macrophages around dying adipocytes (called crown-like structures) correlates with increased levels of pro-inflammatory cytokines in the circulation (Morris et al, 2011), these macrophages have also been considered M1. In conclusion, while there is still some controversy in the field, it is important to consider that macrophages are an heterogeneous population and M1 and M2 are oversimplified extremes. Future work will fully characterize the population of macrophages localized in the breast tissue during obesity.

Equally, the contribution of other immune cells, reported to infiltrate the breast tissue in vivo, remains to be elucidated, together with adipocytes and other stromal cell types, such as fibroblasts.

Finally, our study shows the feasibility of inhibiting IKKe and its downstream signalling, in particular the SBP, as shown by our recent work (https://biorxiv.org/cgi/content/short/855361v1), as preventive strategy to reduce the risk of breast cancer associated with obesity.

Materials and Methods

Reagents and antibodies

All reagents were obtained from Sigma-Aldrich, UK, unless stated otherwise.

Cells

MCF10A cell line (ATCC; LGS Standards UK) was cultured in DMEM/F12 medium supplemented with 5% horse serum (HS), 20 ng/ml epidermal growth factor (EGF), 500 ng/ml hydrocortisone, 10 lg/ml insulin, 100 ng/ml cholera toxin and normocin (InvivoGen, UK). For 3D cultures, the cells were grown in the same medium with reduced HS (2%) and EGF (5 ng/ml) and with an addition of 2% Matrigel (Debnath et al, 2003).

Macrophage differentiation

Peripheral blood mononuclear cells (PBMCs) were isolated from leucocyte cones of healthy deidentified blood donor volunteers from the NHS Blood and Transplant bank, and experiments were conducted in accordance with a protocol approved by Queen Mary Research Ethics Committee (QMREC 2014:61) and in accordance with the Helsinki Declaration. PBMCs were isolated following density gradient centrifugation using Histopaque 1077. These were then plated in 10-cm^2 plate (Greiner) at a density of 2 × 10^7 cells/plate, and monocytes were allowed to adhere to the culture plates for 1 h in PBS (Ca^{2+}/Mg^{2+}). Non-adhering cells were removed with washes with PBS Ca^{2+} and Mg^{2+} free. Monocyte-to-macrophage differentiation was induced for 7 days in RPMI 1640 medium

Downloaded from https://www.embopress.org on April 18, 2024 from IP 147.162.3.230.

supplemented with 10% foetal bovine serum towards either M1-differentiated macrophages (M1D; 50 ng/ml granulocyte–macrophage colony-stimulating factor, GM-CSF; PeproTech) or M2-differentiated macrophage (M2D; 50 ng/ml macrophage colony-stimulating factor, M-CSF; PeproTech). For macrophage activation, M1D macrophages were stimulated with 10 ng/ml LPS (InvivoGen, UK) and 20 ng/ml IFNc for 24 h (M1A), whereas M2D macrophages were stimulated with 20 ng/ml IL-4 for 48 h (M2A) (Martinez et al, 2006; Däbritz et al, 2015; Fig EV1A).

Conditioned medium preparation

Activated or differentiated macrophages were rinsed 4 times with PBS and cultured in DMEM/F12 medium supplemented with 5% HS and normocin for 24 h. The same medium conditioned by MCF10A cells for 24 h was used as control medium. The conditioned medium was collected, filtered (0.45 lm) and stored at 4˚C for up to 1 month.

ELISA

TNF-a (pg/ml) and CCL22 (ng/ml) concentrations were determined in medium conditioned by either macrophages or MCF10A cells (used as control medium) with an ELISA kit according to the manufacturer's instructions (R&D Systems, UK).

Flow cytometry

Macrophages were stained as previously described (Georgouliet al, 2019). Macrophages were washed three times with PBS/, incubated for 5 min at 37° in PBS/ and then gently scraped and washed once with FACS buffer (PBS/, 1% BSA, 2 mM EDTA, 0.1% NaN_3). Non-specific binding sites were blocked with Fc Receptor Blocking Solution (Human TruStain FcX; BioLegend), and then, the cells were co-stained with primary antibodies anti-HLA-DR fluorescein isothiocyanate (FITC)-conjugated (1:50; 11-9952-42; Thermo Fisher Scientific), anti-CD86 phycoerythrin–cyanine 7 (PE-Cy7) (1:20; Clone IT2.2; Thermo Fisher Scientific), anti-CD163 allophycocyanin (APC)-conjugated (1:20; 17-1639-42; Thermo Fisher Scientific) and anti-CD206 PE-conjugated (1:20; Clone 15-2; BioLegend) for 30 min at 4°C in the dark. Cells were washed twice with FACS buffer and stained with DAPI (5 lg/ml) for live/dead cell separation immediately before data acquisition on BD LSRFortessa 1 flow cytometer (BD Biosciences). The data were analysed using FlowJo 10.6.1 software (Tree Star, Inc).

Cytokine array

Cytokines from medium conditioned either by macrophages or MCF10A cells were analysed with human cytokine antibody array (ab133997; Abcam) according to the manufacturer's instructions. Uncultured media were tested to assess baseline signal responses. Signals were detected with chemiluminescence reaction, and densitometry analysis was performed with ImageJ software (https://imagej.nih.gov/ij/).

Proliferation assay

MCF10A cells were plated in 96-well plates (Corning) at a density 1,000 cells per well. Cell proliferation was determined by measuring cell confluence over 5 days using the IncuCyte ZOOM instrument (Essen BioScience, Ann Arbor, MI, USA) and analysed with the IncuCyte ZOOM 2015A software.

Wound-healing assay

MCF10A cells were plated in 96-well plates (IncuCyte ImageLock Plates; Essen BioScience, UK) at a density 50,000 cells per well and grown ON until confluent. To block proliferation, the cells were treated with mitomycin C (10 lg/ml) for 2 h and wounds were made with a 96-pin WoundMaker (Essen BioScience). Cell migration was determined by measuring cell confluency within the wound region over 2 days using the IncuCyte ZOOM instrument (Essen BioScience, Ann Arbor, MI, USA) and analysed with the IncuCyte ZOOM 2015A software.

CRISPR cell line generation

CRISPR-Cas9 system was used to target either IKBKE (crRNA-495656, Dharmacon™; crRNA IKKe) or PHGDH gene (crRNA-497793; Dharmacon™; crRNA PHGDH) in MCF10A cells stably expressing Cas9 (a generous gift from Hyojin Kim, FeiFei Song and Chris Lord ICR—London, UK). MCF10A-Cas9 cells were seeded at a density of 1.5×10^5 cells per 6-cm-diameter well (Corning). On the following day, cells were transfected with crRNA IKKe, crRNA PHGDH or control non-targeting crRNA. The crRNA was mixed with tracrRNA in a 1:1 ratio (2 lM) and then incubated with Opti-MEM (Thermo Fisher Scientific) in a 1:3 ratio for 5 min at RT. RNaiMAX Lipofectamine (Thermo Fisher Scientific)/Opti-MEM mix (1:19 ratio) was prepared independently. CrRNA:tracrRNA mix was added dropwise to Lipofectamine/Opti-MEM mix for a final concentration of crRNA:tracrRNA of 50 nM and left for 20 min at RT. Transfection mix was added dropwise to the MCF10A-Cas9 cells and incubated for 6 h at 37°C. After that, the cells were rinsed with PBS and further cultured for 4 days in the growth medium. Clonal selection was performed by plating single cells in individual wells of a 96-well plate (Corning). Growing colonies were expanded to 12-well plate format and checked for either IKKe or PHGDH expression by Western blotting. Cells with either IKKe or PHGDH knockout or cultures derived from single clones of MCF10A-Cas9 cells treated with control non-targeting crRNA were used for further analyses. To avoid confounding effects of single-cell clones, we combined together 3 clones for each condition (control, IKKe and PHGDH) that were further used as pools.

Western blotting

For Western blot analyses, cells were lysed in a cold lysis buffer (20 mM Tris–HCl, pH 7.4, 135 mM NaCl, 1.5 mM $MgCl_2$, 1% Triton, 10% glycerol) containing protease (Roche, UK) and phosphatase (Thermo Fisher Scientific) inhibitor cocktails. Protein content was quantified, and equal amounts (20 lg) prepared in NuPAGE LDS sample buffer (Thermo Fisher Scientific) were separated by SDS–PAGE using 4–12% NuPAGE™ Bis–Tris Protein gels (Thermo Fisher Scientific). After that, proteins were transferred to Immobilon-P PVDF 0.45 lm membrane (Merck). Protein was detected using primary antibodies anti-IKKε (1:1,000; 14907; Sigma), anti-TBK1 (1:1,000; 3013; Cell Signaling), anti-PHGDH

Downloaded from https://www.embopress.org on April 18, 2024 from IP 147.162.3.230.

ª 2020 The Authors

(1:4,000; HPA021241; Sigma) or anti-actin (1:2,000; sc-1615; Santa Cruz). Enhanced chemiluminescence (Thermo Fisher Scientific) was used for signal detection.

3D invasion assay

MCF10A cells were plated in Matrigel:Collagen I to model the extracellular microenvironment in which Matrigel represents the basement membrane, whereas collagen models the stromal extracellular matrix (Nguyen-Ngoc et al, 2012). 3D culture was assayed as previously described (Arnandis & Godinho, 2015). MCF10A cells were plated in 8-well chamber slides (BD Biosciences) at a density of 10,000 cells per chamber. For IKKe or PHGDH CRISPR-Cas9 knockout or CRISPR-Cas9 control MCF10A cells, individual clones (n = 3) were combined in equal ratio prior seeding in the gels. Growth factor-reduced Matrigel was used (BD Biosciences) with a protein concentration between 9 and 11 mg/ml. Collagen (Corning) was used at the concentration 1.2 mg/ml. MCF10A cells were cultured in the assay medium with reduced HS (2%) and EGF (5 ng/ml) and 2% Matrigel (Godinho et al, 2014) with medium replaced every 4 days. On day 16, MCF10A spheroids were stimulated with either macrophage-conditioned or control medium supplemented with 20 ng/ml EGF, 500 ng/ml hydrocortisone and 10 lg/ml insulin. For IKKe inhibition, MCF10A spheroids were stimulated with conditioned medium in the presence of specific inhibitor of IKKe/TBK1-amlexanox (50 lM; Abcam) (Reilly et al, 2013). To inhibit the serine biosynthesis pathway, the PHGDH inhibitor NCT502 (10 lM; Cayman) was used (Pacold et al, 2016). For Rac1 inhibition, the spheroids were treated with NSC23766 (50 lM; EMD Millipore) (Godinho et al, 2014). After 24 h, invasion was quantified microscopically by visual scoring.

Immunofluorescence microscopy on 3D cultures

MCF10A spheroids were fixed and stained as previously described (Arnandis & Godinho, 2015). Spheroids were washed in PBS and fixed with 4% PFA (Thermo Fisher Scientific) in PBS for 20 min at 37°C. Then, the spheroids were rinsed with PBS:glycine (100 mM) in PBS 3 times for 10 min each and permeabilized with 0.5% Triton X-100 for 10 min. Permeabilized spheroids were rinsed for 10 min with 10% FBS in immunofluorescence buffer (IF; 130 mM NaCl, 13 mM Na_2HPO_4, 3.5 mM NaH_2PO_4, 7.7 mM NaN_3, 0.1% bovine serum albumin, 0.2% Triton X-100, 0.05% Tween-20 at pH 7.4) and blocked with 10% FBS-IF buffer for 1 h. Then, the spheroids were incubated with primary antibodies anti-Laminin V Alexa 488-conjugated (1:200; Millipore) or anti-Ki67 Alexa 488-conjugated (1:100, BD Pharmingen) in 10% FBS-IF buffer ON at 4°C. Spheroids were washed with IF buffer three times for 20 min each and then incubated with Alexa Fluor 633 phalloidin for b-actin staining (1:500; Thermo Fisher Scientific) for 1 h in 10% FBS-IF buffer. The spheroids were rinsed 3 times for 10 min and stained for DNA with Hoechst 33342 (1:2,500, BD Pharmingen) for 5 min, and washed with PBS for 10 min. 3D cultures were mounted in ProLong Gold Antifade mounting medium (Thermo Fisher Scientific). The spheroids were analysed under Zeiss LSM 710 confocal microscope (Carl Zeiss Microscopy, U.S.) using Zen 2009 software. For quantification of lumen filling, at least 50 spheroids in duplicate were scored per condition for each experiment according to the criteria for lumen filling with cell nuclei: filled (~90–100% filled), almost filled (~50–90% filled), partially filled (~10–50% filled) and clear (~0–10% filled) as shown in Fig 1B. For Ki67 staining analysis, the percentage of Ki67-positive nuclei/spheroid was determined.

Soft agar assay

MCF10A, IKKe or PHGDH CRISPR-Cas9 knockout MCF10A cells, or CRISPR-Cas9 MCF10A control cells were seeded in 0.4% soft agar in macrophage-conditioned or control medium on a layer of 0.6% soft agar in the same medium in 24-well plate (Corning) at a density of 5,000 cells per well (n = 3 per condition). For IKKe or PHGDH CRISPR-Cas9 knockout or CRISPR-Cas9 control cells, individual clones (n = 3) were combined in equal ratio prior seeding in soft agar. Cultures were fed every 7 days with 0.4% soft agar in the same medium. For IKKe inhibition, amlexanox (50 lM) was added to the medium. To inhibit serine biosynthesis pathways, NCT502 (10 lM) was added to the medium. After 5 weeks, colonies greater than 50 lm in diameter were quantified microscopically.

Organoids

Mammary organoids from 19- to 20-week-old C57Bl/6 mice that were either on high-fat diet (HFD; body weight: 27.2 g 1.48) or normal diet (ND; body weight: 21.3 g 1.27) were isolated and plated for 3D cultures as previously described (Nguyen-Ngoc et al, 2015) (n = 3 per group). Briefly, fat pads were minced and then enzymatically digested in collagenase solution in DMEM/F12 medium (2 mg/ml collagenase, 2 mg/ml trypsin, 5% FBS, 5 lg/ml insulin and 50 lg/ml gentamicin) for 40–50 min at 37°C on a shaker (130 rpm). Organoid suspension was treated with 2 U/ll DNase for 5 min to detach organoids from single cells, and organoids were purified from stromal cell populations by differential centrifugation (176 g for 3–4 s, × 4 spins). Isolated organoids were assayed in two different culture set-ups of extracellular matrix and were plated either in Matrigel:Collagen I or Collagen I in 8-well chamber slides (BD Biosciences).

Organoids: Invasion assay in Collagen/Matrigel

Organoids were plated at a density of 1.8 organoids per 1 ll of Matrigel:Collagen I. Collagen was used at the concentration 2.4 mg/ml. Organoids were cultured in DMEM/F12 medium supplemented with 1% insulin–transferrin–selenium– X (ITS, Gibco), 2.5 nM fibroblast growth factor 2 (FGF2) and 1% penicillin/streptomycin. After 2 days, the organoids were stimulated with either macrophage-conditioned or control medium supplemented with 1% ITS and 2.5 nM FGF2. Amlexanox (50 lM) was used to inhibit IKKe (Reilly et al, 2013). NCT502 (10 lM) was used to inhibit PHGDH (Pacold et al, 2016). After 24 h, invasion was quantified microscopically.

Organoids: Invasion assay in collagen

Previous studies reported that collagen I induces in both normal and tumour organoids, a conserved response of protrusive invasion (Nguyen-Ngoc et al, 2012). To test possible differences in responses of protrusive invasion between HFD and ND organoids, organoids

Downloaded from https://www.embopress.org on April 18, 2024 from IP 147.162.3.230.

ª 2020 The Authors

were assayed in Collagen I. Organoids were plated at a density of 1.8 organoids per 1 ll of Collagen I (3 mg/ml) and cultured in DMEM/F12 medium supplemented with 1% ITS, 2.5 nM FGF2 and 1% penicillin/streptomycin ON. Amlexanox (50 lM) or NCT502 (10 lM) was added to the culture medium for further 24 h. Then, the number of invasive protrusions per each organoid was quantified microscopically with 30 organoids scored per condition.

Organoids: Immunofluorescence microscopy

Organoids were fixed and stained as previously described (Nguyen-Ngoc et al, 2015). Briefly, organoids were washed in PBS and fixed with 4% PFA in PBS for 15 min at RT. Then, the organoids were washed in PBS 3 times for 10 min each and permeabilized with 0.5% Triton X-100 for 40 min. Permeabilized organoids were blocked with 10% FBS in PBS for 2 h and then incubated with anti-a-SMA antibody (1:200) in 10% FBS-PBS ON at 4°C. Organoids were washed with 10% FBS-PBS 3 times for 10 min each and incubated with Alexa 488-conjugated secondary antibody (1:500; Thermo Fisher Scientific) and Alexa Fluor 633 phalloidin (1:500) for 1 h in 10% FBS-PBS. The spheroids were washed in PBS 3 times for 10 min and incubated with Hoechst 33342 (1:2,500) for 5 min, and washed with PBS for 10 min.

3D cultures were mounted in ProLong Gold Antifade mounting medium (Thermo Fisher Scientific). The spheroids were analysed under Zeiss LSM 710 confocal microscope (Carl Zeiss Microscopy, U.S.) using Zen 2009 software.

3D ductal culture

Myoepithelial and luminal cells isolated from human breast tissue were previously shown to reform ductal structures with internal luminal cell layer and external myoepithelial cell layer, and with luminal compartment when grown in collagen gels (Carter et al, 2017). Furthermore, in the same model, inducible expression of HER2 in luminal compartment was shown to induce luminal filling, recapitulating ductal carcinoma in situ. Thus, this 3D model appears to recreate physiologically reflective duct (Carter et al, 2017).

Pure populations of myoepithelial and luminal cells (n = 2) were obtained from the Breast Cancer Now Tissue Bank at the Barts Cancer Institute (REC:15/EE/0192). All patients donated tissues from which cells were derived following fully informed consent, and all experiments conformed to the principles set out in the WMA Declaration of Helsinki and the Department of Health and Human Services Belmont Report. Luminal cells were cultured in DMEM/F12 medium supplemented with 10% FBS, 0.5 lg/ml hydrocortisone, 10 lg/ml apo-transferrin, 5 lg/ml insulin and 10 ng/ml EGF. Myoepithelial cells were cultured in HuMEC medium (Thermo Fisher Scientific) supplemented with 0.5 lg/ml hydrocortisone, 5 lg/ml insulin, 10 ng/ml EGF and 50 lg/ml bovine pituitary extract (Thermo Fisher Scientific; Carter et al, 2017).

3D ducts: lumen filling assay

Myoepithelial and luminal cells were combined in a 1:1 ratio (1 × 10^4 cells each) and seeded into 2 mg/ml collagen I type gels as previously described (Carter et al, 2017). Cells were grown for 14 days to reform ductal structures in luminal culture medium with medium replaced every 2-3 days. From day 14, 3D ducts were cultured in macrophage (M1A or M2A)- or MCF10A-conditioned medium supplemented as the luminal culture medium. Amlexanox (50 lM) was used to inhibit IKKe (Reilly et al, 2013). NCT502 (10 lM) was used to inhibit PHGDH (Pacold et al, 2016).

3D ducts: Immunofluorescence microscopy

3D ducts were fixed and stained as previously described (Carter et al, 2017). Briefly, the collagen gels were treated with 1 mg/ml collagenase, and then, the ducts were fixed with 10% neutral-buffered formalin for 10 min at 37°C and then permeabilized ON with 1% Triton X-100 and blocked in 10% FBS/2%BSA. The gels were incubated with 1 lM Alexa Fluor 564 phalloidin for b-actin staining (A22283, Thermo Fisher Scientific) for 10 min and stained for DNA with 1 lg/ml DAPI prior to mounting.

Fluorescent images were acquired using Zeiss LSM 710 confocal microscope (Carl Zeiss Microscopy, U.S.). For quantification of lumen filling, 3 ducts in duplicate were scored per each condition according to previously described eight-step image analysis process (Carter et al, 2017). For each 3D duct, raw DAPI-labelled z-sections were analysed to calculate the total area of the sphere and the area of luminal space in the centre. Filling of the lumen was determined as % of luminal space filled with cells.

Mouse models

Female C57Bl/6 mice heterozygous for the polyomavirus middle T antigen (PyMT) under the control of the mouse mammary tumour virus promoter (MMTV) started high-fat diet (HFD; 45% of calories come from fat: TestDiet) at 6–7 weeks of age, in parallel to mice on normal diet (ND; 15% of calories come from fat: LabDiet). A week after starting the diet, the mice were administered amlexanox (25 mg per kg body weight, 17 mM) (Reilly et al, 2013) or vehicle control (250 mM Tris, 45 mM NaOH, pH 7.5) daily by oral gavage. The appearance of new tumours was monitored twice per week. A control diet group (wild-type mice) was included to confirm the efficacy of the diet and to control for possible unpredicted interactions of the MMTV-PyMT gene. The body weight of the mice was measured once per week.

To quantify adipocyte diameter, mammary fat pads were fixed in 10% formalin, paraffin-embedded, sectioned (4 lm), fixed on slides and H&E-stained. Average adipocyte diameter was calculated by measuring the major diameter of at least 100 adipocytes per mice using AxioVision software 4.8 (Zeiss).

To quantify macrophage infiltration in mammary fat pads, tissue sections fixed on slides were processed for immunohistochemistry (IHC) using standard IHC procedures. Briefly, antigen retrieval was performed by enzymatic digestion using protease 1 (Roche, UK), tissue sections were stained for a macrophage marker with rat anti-F4/80 antibody (1:300; Bio-Rad, UK), and the staining was visualized with DAB (Vector Laboratories, UK) reaction. The number of macrophages was determined by counting F4/80 + macrophages in at least 10 fields of view (depending on tissue availability) and averaged per each mouse.

All animal procedures were approved by the animal ethics committee of Queen Mary of London and were performed in accordance with United Kingdom Home Office regulations.

Downloaded from https://www.embopress.org on April 18, 2024 from IP 147.162.3.230.

ª 2020 The Authors

Immunohistochemistry

Breast tissue samples from 66 female patients diagnosed with primary breast carcinoma between the period 2013 and 2016 were obtained from the BCI Breast Tissue Bank (Ethics Ref: 15/EE/0192). All patients donated tissue following fully informed consent, and all experiments conformed to the principles set out in the WMA Declaration of Helsinki and the Department of Health and Human Services Belmont Report. The patients were of mixed race and ethnicity with the white British as a largest group (38%). The mean age of the patients was 60.6 years 12.8 SD, and 79% of patients were post-menopause.

Tumours were characterized by invasive tumour grade and size. According to the invasive grade status, 56% of tumours were classified as grade 3 tumours, 35% as grade 2 and 9% as grade 1. Average tumour size was 24 mm 14.8 SD. To determine IKKe expression, tumours were fixed in 10% formalin, paraffin-embedded, sectioned (4 lm) and fixed on slides. Tissue sections were processed for IHC using standard IHC procedures. Briefly, antigen retrieval was performed by boiling tissue sections in microwave in antigen unmasking solution, citric acid-based (Vector Laboratories, UK). Tissue sections were stained for IKKe with rabbit anti-IKKe C-terminal (1:400; SAB1306435; Sigma), and the staining was visualized with DAB (Vector Laboratories, UK) reaction. To determine PSAT1 expression (n = 41), tissue sections were processed for IHC using Ventana DiscoveryXT automated slide staining system (Roche, UK). Tissue sections were stained for PSAT1 with rabbit anti-PSAT1 (1:50; 20180-1-AP; Proteintech, UK), and the staining was visualized with DAB reaction (Roche, UK). Protein expression was assessed semi-quantitatively using a 0-3 grade scale ("0": no staining; "1": weak staining; "2": moderate staining; "3": strong staining).

The specificity of IKKe antibody for IHC analysis was determined by confirming a positive staining in IKKe expressing breast cancer cell line MDA-MB-468 and the lack of IKKe staining in 293-Flp-In cells that do not express the kinase by IHC. For IHC analysis of PSAT1, the specificity of the PSAT1 antibody was determined in MDA-MB-453 breast cancer cell line with doxycycline-inducible PSAT1 gene.

Immune cell infiltration in the breast tissue was assessed semi-quantitatively by histopathology examination in the sections previously stained by IHC for IKKe using (0–4) inflammation grade ("0": no inflammatory cells; "1": weak inflammation; "2": moderate inflammation; "3": strong inflammation; "4": very strong inflammation).

Gene expression analysis

The METABRIC gene expression dataset (Curtis et al, 2012) was obtained from Synapse: http://www.synapse.org (syn1688369/METABRIC Data for Use in Independent Research). ESTIMATE analysis to predict the presence of stromal/immune cells in tumour tissues was performed using the ESTIMATE R-package version 1.0.13 (http://r-forge.r-project.org/R/?group_id=2237). ESTIMATE algorithm is based on single-sample Gene Set Enrichment Analysis and generates three scores: (1) stromal score (that captures the presence of stroma in tumour tissue), (2) immune score (that represents the infiltration of immune cells in tumour tissue) and (3) estimate score (that infers tumour purity; Yoshihara et al, 2013). Immune scores for each sample were calculated, and correlation to $\log_2$-normalized gene expression was computed using Pearson's method. Correlation values and adjusted r-squared are shown.

Statistics

Statistical analysis was performed using GraphPad Prism 8.0 or R software (version 3.5.0). For parametric data analyses, Student's t-test was used for comparison between two groups or one-way ANOVA with uncorrected Fisher's LSD post hoc test when comparing more than two groups. For in vivo data, to determine the statistical significance between the numbers of developed tumours across all time points, log-rank test was used. To evaluate IKKe expression in breast carcinomas, Kruskal–Wallis test with uncorrected Dunn's post hoc test was used. The associations between protein expression and immune cell infiltration in breast carcinomas were assessed using Spearman's correlation. $P < 0.05$ was considered statistically significant.

Expanded View for this article is available online.

Acknowledgments

The authors wish to acknowledge the role of the Breast Cancer Now Tissue Bank in collecting and making available the tissue and primary cell samples used in the generation of this publication, the Barts Cancer Institute pathology facility and George Elia for help and support during this study, Elzbieta Stankiewicz for help with immunohistochemical staining procedure, Teresa Arnandis for guidance on 3D assays and Tencho Tenev, Hyojin Kim, FeiFei Song and Chris Lord for guidance in the generation of the MCF10A-CRISPR cells. We are grateful to Julie Cleaver and Tracy Chaplin-Perkins from the Animal Technical Service team for helping with mice care and oral gavage during the in vivo study. We thank Shannon Reilly and Alan Saltiel for useful guidance on the use of amlexanox in vivo and Jacek Marzec for helping with statistical analysis. We are also grateful to Mirella Georgouli, Victoria Sanz-Moreno and Agata Krygowska for their guidance in the characterization of macrophages at the FACS. We would like to thank Robert James Hearnden for feedback on this manuscript. KB and EW-V are supported by the Barts London Charity (Grant Reference Number 467/2053). GS is funded by University College London COMPLeX/British Heart Foundation Fund (SP/08/004), BBSRC (BB/L020874/1) and the Wellcome Trust (097815/Z/11/Z) in the UK, and the Italian Association for Cancer Research (AIRC, IG13447). JD is supported by a Sir Henry Dale Fellowship jointly funded by the Wellcome Trust and the Royal Society (grant no. 107613/Z/15/Z). EC and RG are supported by Breast Cancer Now (Grant: 2017NovPR988), and KH-D is funded by CRUK (programme grant C8218/A21453).

Author contributions

EW-V designed and performed the majority of the experiments described in the manuscript. EC and RG conducted and analysed experiment on 3D human duct model. AI analysed mouse tissues. RX performed WB and helped with clonal selection. JM conducted transfection. JH and KH-D helped with the planning and execution of the in vivo experiments. WJ helped with optimization of PSAT1 staining in human tissue. RMB and LU helped with the analysis of mouse tissues. SAG provided support and guidance in establishing the 3D model system with MCF10A and organoids. JD provided support in differentiating macrophages from PBMCs. GS and RBB analysed the METABRIC dataset. LJ analysed and quantified the tissue sections of human breast cancer cases. KB designed the study and wrote the manuscript with the help of EW-V, GS, SAG, KH-D, JD and LJ.

Downloaded from https://www.embopress.org on April 18, 2024 from IP 147.162.3.230.

The paper explained

Problem
Obesity is constantly increasing in developing countries. One in 20 cases of cancer can be attributed to obesity, which is now considered the second most preventable cause of cancer after smoking. In particular, the low level of chronic inflammation associated with obesity is a key factor responsible for the higher risk of cancer development, also in the case of breast tumours, where macrophages infiltrating the breast tissue give rise to an inflammatory response. However, the exact role of macrophages in promoting tumourigenesis remains elusive as well as the mechanism by which they act. Thus, the purpose of our study was to explore the very early stages of breast cancer during obesity and formally investigate the mechanisms by which macrophages promote tumourigenesis.

Results
Our data demonstrate that medium conditioned by macrophages derived from human healthy donors induces acquisition of a malignant phenotype in different 3D systems: (i) the non-transformed MCF10A cells, (ii) mouse primary organoids and (iii) human primary breast epithelial cells derived from patients. This transforming effect of macrophages is prevented by the FDA-approved drug amlexanox, inhibitor of the innate immunity kinases IKKe/TBK1 and also by genetic inhibition of IKKe (via CRISPR/Cas9). Furthermore, in line with the role of IKKe as regulator of the serine biosynthesis pathway, we show that the inhibition of this pathway via the newly developed compound NCT502 (targeting PHGDH) prevents macrophage-induced transformation as well as deletion of PHGDH gene via CRISPR/Cas9. Amlexanox delays tumour appearance in a combined genetic mouse model of breast cancer and high-fat diet-induced obesity/inflammation in vivo. We also validated the link between inflammation–IKKe and alteration of cellular metabolism further in translational studies. We show a positive correlation between IKKe expression, immune cell infiltration and the expression of the serine biosynthesis pathway enzyme PSAT1 in human breast cancer tissues and in the METABRIC breast cancer dataset.

Impact
Here, we describe a mechanism linking macrophage-mediated activation of the innate immune system to the very early stages of malignant transformation of breast epithelial cells. We show that macrophages derived from human healthy donors promote malignant transformation. Moreover, inhibition of either the innate immune kinases IKKe/TBK1 or the serine biosynthesis pathway prevents the phenotype. Since amlexanox safety has been confirmed in human patients, we propose that this drug is an interesting candidate to be tested in preventive therapeutic strategies, aiming to reduce the risk of breast cancer associated with obesity.

Conflict of interest

The authors declare that they have no conflict of interest.

References

Agnoli C, Berrino F, Abagnato CA, Muti P, Panico S, Crosignani P, Krogh V (2010) Metabolic syndrome and postmenopausal breast cancer in the ORDET cohort: a nested case-control study. Nutr Metab Cardiovasc Dis 20: 41 – 48

Arendt LM, McCready J, Keller PJ, Baker DD, Naber SP, Seewaldt V, Kuperwasser C (2013) Obesity promotes breast cancer by CCL2-mediated macrophage recruitment and angiogenesis. Cancer Res 73: 6080 – 6093

Arnandis T, Godinho SA (2015) Studying centrosome function using three-dimensional cell cultures. Methods Cell Biol 129: 37 – 50

Barbie TU, Alexe G, Aref AR, Li S, Zhu Z, Zhang X, Imamura Y, Thai TC, Huang Y, Bowden M et al (2014) Targeting an IKBKE cytokine network impairs triple-negative breast cancer growth. J Clin Invest 124: 5411 – 5423

Boehm JS, Zhao JJ, Yao J, Kim SY, Firestein R, Dunn IF, Sjostrom SK, Garraway LA, Weremowicz S, Richardson AL et al (2007) Integrative genomic approaches identify IKBKE as a breast cancer oncogene. Cell 129: 1065 – 1079

Borowicz S, Van Scoyk M, Avasarala S, Karuppusamy Rathinam MK, Tauler J, Bikkavilli RK, Winn RA (2014) The soft agar colony formation assay. J Vis Exp 51998

Bowers LW, Maximo IXF, Brenner AJ, Beeram M, Hursting SD, Price RS, Tekmal RR, Jolly CA, DeGraffenried LA (2014) NSAID use reduces breast cancer recurrence in overweight and obese women: role of prostaglandin-aromatase interactions. Cancer Res 74: 4446 – 4457

Calle EE, Rodriguez C, Walker-Thurmond K, Thun MJ (2003) Overweight, obesity, and mortality from cancer in a prospectively studied cohort of U.S. adults. N Engl J Med 348: 1625 – 1638

Carter EP, Gopsill JA, Gomm JJ, Jones JL, Grose RP (2017) A 3D in vitro model of the human breast duct: a method to unravel myoepithelial-luminal interactions in the progression of breast cancer. Breast Cancer Res 19: 1 – 10

Chiang S-H, Bazuine M, Lumeng CN, Geletka LM, Mowers J, White NM, Ma J-T, Zhou J, Qi N, Westcott D et al (2009) The protein kinase IKKepsilon regulates energy balance in obese mice. Cell 138: 961 – 975

Cowen S, Mclaughlin SL, Hobbs G, Coad J, Martin KH, Olfert MI, Vona-Davis L (2015) High-fat, high-calorie diet enhances mammary carcinogenesis and local inflammation in mmtv-pymt mouse model of breast cancer. Cancers (Basel) 7: 1125 – 1142

Cranford TL, Velázquez KT, Enos RT, Bader JE, Carson MS, Chatzistamou I, Nagarkatti M, Murphy EA (2017) Loss of monocyte chemoattractant protein-1 expression delays mammary tumorigenesis and reduces localized inflammation in the C3(1)/SV40Tag triple negative breast cancer model. Cancer Biol Ther 18: 85 – 93

Curtis C, Shah SP, Chin S-F, Turashvili G, Rueda OM, Dunning MJ, Speed D, Lynch AG, Samarajiwa S, Yuan Y et al (2012) The genomic and transcriptomic architecture of 2,000 breast tumours reveals novel subgroups. Nature 486: 346 – 352

Däbritz J, Weinhage T, Varga G, Wirth T, Walscheid K, Brockhausen A, Schwarzmaier D, Brückner M, Ross M, Bettenworth D et al (2015) Reprogramming of monocytes by GM-CSF contributes to regulatory immune functions during intestinal inflammation. J Immunol 194: 2424 – 2438

Debnath J, Muthuswamy SK, Brugge JS (2003) Morphogenesis and oncogenesis of MCF-10A mammary epithelial acini grown in three-dimensional basement membrane cultures. Methods 30: 256 – 268

Debnath J, Brugge JS (2005) Modelling glandular epithelial cancers in three-dimensional cultures. Nat Rev Cancer 5: 675 – 688

Deng T, Liu JC, Chung PED, Uehling D, Aman A, Joseph B, Ketela T, Jiang Z, Schachter NF, Rottapel R et al (2014) ShRNA kinome screen identifies TBK1 as a therapeutic target for HER2 + breast cancer. Cancer Res 74: 2119 – 2130

Gao Y, Dickerson JB, Guo F, Zheng J, Zheng Y (2004) Rational design and characterization of a Rac GTPase-specific small molecule inhibitor. Proc Natl Acad Sci USA 101: 7618 – 7623

Downloaded from https://www.embopress.org on April 18, 2024 from IP 147.162.3.230.

 ª 2020 The Authors

Georgouli M, Herraiz C, Crosas-Molist E, Fanshawe B, Maiques O, Perdrix A, Pandya P, Rodriguez-Hernandez I, Ilieva KM, Cantelli G et al (2019) Regional activation of myosin II in cancer cells drives tumor progression via a secretory cross-talk with the immune microenvironment. Cell 176: 757 – 774.e23
Godinho SA, Picone R, Burute M, Dagher R, Su Y, Leung CT, Polyak K, Brugge JS, Théry M, Pellman D (2014) Oncogene-like induction of cellular invasion from centrosome amplification. Nature 510: 167 – 171.
Incio J, Ligibel JA, Mcmanus DT, Suboj P, Jung K, Kawaguchi K, Pinter M, Babykutty S, Chin SM, Vardam TD et al (2018) Obesity promotes resistance to anti-VEGF therapy in breast cancer by up-regulating IL-6 and potentially FGF-2. Sci Transl Med 10: eaag0945
Jablonski KA, Amici SA, Webb LM, Ruiz-Rosado JDD, Popovich PG, Partida-Sanchez S, Guerau-De-arellano M (2015) Novel markers to delineate murine M1 and M2 macrophages. PLoS ONE 10: 5 – 11
Janda E, Litos G, Grünert S, Downward J, Beug H (2002) Oncogenic Ras/Her-2 mediate hyperproliferation of polarized epithelial cells in 3D cultures and rapid tumor growth via the PI3K pathway. Oncogene 21: 5148 – 5159
Leung CT, Brugge JS (2012) Outgrowth of single oncogene-expressing cells from suppressive epithelial environments. Nature 482: 410 – 413
Locasale JW, Grassian AR, Melman T, Lyssiotis CA, Mattaini KR, Bass AJ, Heffron G, Metallo CM, Muranen T, Sharfi H et al (2011) Phosphoglycerate dehydrogenase diverts glycolytic flux and contributes to oncogenesis. Nat Genet 43: 869 – 874
Locasale JW (2013) Serine, glycine and one-carbon units: cancer metabolism in full circle. Nat Rev Cancer 13: 572 – 583
Martinez FO, Gordon S, Locati M, Mantovani A (2006) Transcriptional profiling of the human monocyte-to-macrophage differentiation and polarization: new molecules and patterns of gene expression. J Immunol 177: 7303 – 7311
Morris PG, Hudis CA, Giri D, Morrow M, Falcone DJ, Zhou XK, Du B, Brogi E, Crawford CB, Kopelovich L et al (2011) Inflammation and increased aromatase expression occur in the breast tissue of obese women with breast cancer. Cancer Prev Res 4: 1021 – 1029
Murray PJ, Wynn TA (2011) Protective and pathogenic functions of macrophage subsets. Nat Rev Immunol 11: 723 – 737
Muthuswamy SK, Li D, Lelievre S, Bissell MJ, Brugge JS (2001) ErbB2, but not ErbB1, reinitiates proliferation and induces luminal repopulation in epithelial acini. Nat Cell Biol 3: 785 – 792
Nguyen-Ngoc K-V, Cheung KJ, Brenot A, Shamir ER, Gray RS, Hines WC, Yaswen P, Werb Z, Ewald AJ (2012) ECM microenvironment regulates collective migration and local dissemination in normal and malignant mammary epithelium. Proc Natl Acad Sci 109: E2595 – E2604
Nguyen-Ngoc K-V, Shamir ER, Huebner RJ, Beck JN, Cheung KJ, Ewald AJ (2015) 3D culture assays of murine mammary branching morphogenesis and epithelial invasion. Methods Mol Biol 1189: 135 – 162
tenOever BR, Ng S-L, Chua MA, McWhirter SM, Garcia-Sastre A, Maniatis T (2007) Multiple Functions of the IKK-Related Kinase IKK in Interferon-Mediated Antiviral Immunity. Science 315: 1274 – 1278
Olefsky JM (2009) IKKe: Bridge between Obesity and Inflammation. Cell 138: 834– 836
Olson OC, Quail DF, Joyce JA (2017) Obesity and the tumor microenvironment. Science 358: 1130 – 1131
Oral EA, Reilly SM, Gomez AV, Meral R, Butz L, Ajluni N, Chenevert TL, Korytnaya E, Neidert AH, Hench R et al (2017) Inhibition of IKKε and TBK1 improves glucose control in a subset of patients with type 2 diabetes. Cell Metab 26: 157 – 170.e7
Pacold ME, Brimacombe KR, Chan SH, Rohde JM, Lewis CA, Swier LJYM, Possemato R, Chen WW, Sullivan LB, Fiske BP et al (2016) A PHGDH inhibitor reveals coordination of serine synthesis and one-carbon unit fate. Nat Chem Biol 12: 452 – 458
Possemato R, Marks KM, Shaul YD, Pacold ME, Kim D, Birsoy K, Sethumadhavan S, Woo H-K, Jang HG, Jha AK et al (2011) Functional genomics reveal that the serine synthesis pathway is essential in breast cancer. Nature 476: 346 – 350
Reilly SM, Chiang S-H, Decker SJ, Chang L, Uhm M, Larsen MJ, Rubin JR, Mowers J, White NM, Hochberg I et al (2013) An inhibitor of the protein kinases TBK1 and IKK-ε improves obesity-related metabolic dysfunctions in mice. Nat Med 19: 313 – 321
Sanada Y, Kumoto T, Suehiro H, Yamamoto T, Nishimura F, Kato N, Yanaka N (2014) IjB kinase epsilon expression in adipocytes is upregulated by interaction with macrophages. Biosci Biotechnol Biochem 78: 1357 – 1362
Schafer ZT, Grassian AR, Song L, Jiang Z, Gerhart-Hines Z, Irie HY, Gao S, Puigserver P, Brugge JS (2009) Antioxidant and oncogene rescue of metabolic defects caused by loss of matrix attachment. Nature 461: 109 – 113
Scholzen T, Gerdes J (2000) The Ki-67 protein: from the known and the unknown. J Cell Physiol 182: 311 – 322
Seo BR, Bhardwaj P, Choi S, Gonzalez J, Eguiluz RCA, Wang K, Mohanan S, Morris PG, Du B, Zhou XK et al (2015) Obesity-dependent changes in interstitial ECM mechanics promote breast tumorigenesis. Sci Transl Med 7: 301ra130
Shimada T, Kawai T, Takeda K, Matsumoto M, Inoue J, Tatsumi Y, Kanamaru A, Akira S (1999) IKK-i, a novel lipopolysaccharide-inducible kinase that is related to IkappaB kinases. Int Immunol 11: 1357 – 1362
Springer NL, Iyengar NM, Bareja R, Verma A, Jochelson M, Giri DD, Zhou XK, Elemento O, Dannenberg AJ, Fischbach C (2019) Obesity-associated extracellular matrix remodeling promotes a macrophage phenotype similar to tumor-associated macrophages. Am J Pathol 189: 2019 – 2035
Stefan N, Schick F, Häring HU (2017) Causes, characteristics, and consequences of metabolically unhealthy normal weight in humans. Cell Metab 26: 292 – 300
Subbaramaiah K, Howe LR, Bhardwaj P, Du B, Gravaghi C, Yantiss RK, Zhou XK, Blaho VA, Hla T, Yang P et al (2011) Obesity is associated with inflammation and elevated aromatase expression in the mouse mammary gland. Cancer Prev Res 4: 329 – 346
Sun X, Casbas-Hernandez P, Bigelow C, Makowski L, Joseph Jerry D, Smith Schneider S, Troester MA (2012) Normal breast tissue of obese women is enriched for macrophage markers and macrophage-associated gene expression. Breast Cancer Res Treat 131: 1003 – 1012
Tiwari P, Blank A, Cui C, Schoenfelt KQ, Zhou G, Xu Y, Khramtsova G, Olopade F, Shah AM, Khan SA et al (2019) Metabolically activated adipose tissue macrophages link obesity to triple-negative breast cancer. J Exp Med 216: 1345 – 1358
Wang SE, Shin I, Wu FY, Friedman DB, Arteaga CL (2006) HER2/Neu (ErbB2) signaling to Rac1-Pak1 is temporally and spatially modulated by transforming growth factor b. Cancer Res 66: 9591 – 9600
Williams CB, Yeh ES, Soloff AC (2016) Tumor-associated macrophages: unwitting accomplices in breast cancer malignancy. NPJ Breast Cancer 2: 15025
Wolford CC, McConoughey SJ, Jalgaonkar SP, Leon M, Merchant AS, Dominick JL, Yin X, Chang Y, Zmuda EJ, O'Toole SA et al (2013) Transcription factor ATF3 links host adaptive response to breast cancer metastasis. J Clin Invest 123: 2893 – 2906
Yang XR, Chang-Claude J, Goode EL, Couch FJ, Nevanlinna H, Milne RL, Gaudet M, Schmidt MK, Broeks A, Cox A et al (2011) Associations of breast cancer risk factors with tumor subtypes: a pooled analysis from the breast cancer association consortium studies. J Natl Cancer Inst 103: 250 – 263

Downloaded from https://www.embopress.org on April 18, 2024 from IP 147.162.3.230.

ª 2020 The Authors

Yang KM, Jung YS, Lee JM, Kim WJ, Cho JK, Jeong J, Kim SJ (2013) Loss of TBK1 induces epithelial-mesenchymal transition in the breast cancer cells by ERa downregulation. Cancer Res 73: 6679 – 6689
Yang M, Vousden KH (2016) Serine and one-carbon metabolism in cancer. Nat Rev Cancer 16: 650 – 662
Yoshihara K, Shahmoradgoli M, Martínez E, Vegesna R, Kim H, Torres-Garcia W, Treviño V, Shen H, Laird PW, Levine DA et al (2013) Inferring tumour purity and stromal and immune cell admixture from expression data. Nat Commun 4: 2612
Zahir N, Lakins JN, Russell A, Ming WY, Chatterjee C, Rozenberg GI, Marinkovich MP, Weaver VM (2003) Autocrine laminin-5 ligates a6b4 integrin and activates RAC and NFjB to mediate anchorage-independent survival of mammary tumors. J Cell Biol 163: 1397 – 1407
Zhao P, Wong KI, Sun X, Reilly SM, Uhm M, Liao Z, Skorobogatko Y, Saltiel AR (2018) TBK1 at the crossroads of inflammation and energy homeostasis in adipose tissue. Cell 172: 731 – 743.e12

License: This is an open access article under the terms of the Creative Commons Attribution 4.0 License, which permits use, distribution and reproduction in any medium, provided the original work is properly cited.

Downloaded from https://www.embopress.org on April 18, 2024 from IP 147.162.3.230.

ª 2020 The Authors